ADDIS ABABA UNIVERSITY

SCHOOL OF GRADUATE STUDIES

DEPARTMENT OF CIVIL AND ENVIRMONATLA ENGINEERING

Urban Landscape Dynamics and the Implication on Surface Urban Heat Island: The Case of Hawassa Town and Surrounding Area, Ethiopia

By:

Mohammed Habtamu Seid

By the supervision of: - Dr. Berhan Gessesse (Associate Professor)

A thesis submitted to the School of Graduate School of Addis Ababa University in the partial fulfillment of the requirements for the Degree of Master of Science in Geodesy and Geomatics specialized by Geomatics.

November, 2018

ADDIS ABABA, ETHIOPIA

C E R T I F I C A T E

This is certified that the dissertation entitled "**Urban Landscape Dynamics and Its Implication on Surface Urban Heat Island: The Case of Hawassa Town and Surrounding Area, Ethiopia**" is a bonafiled work carried out by Mohammed Habtamu Seid under my guidance and supervision. This is the actual work done by Mohammed Habtamu Seid for the partial fulfillment of the award of the Degree of Master of Science in Geodesy and Geomatics specialized By Geomatics.

Dr. Berhan Gessesse

Associate Professor

Department of Civil and Environmental Science

Addis Ababa

ADDIS ABABA UNIVERSITY

SCHOOL OF GRADUATE STUDIES

DEPARTMENT OF CIVIL AND ENVIRMONATLA ENGINEERING

Urban Landscape Dynamics and Its Implication on Surface Urban Heat Island:

The Case of Hawassa Town and Surrounding Area, Ethiopia

By

Mohammed Habtamu

Approved by board of examiners:

_____	_____	_____
Advisor	Signature	Date
_____	_____	_____
Internal Examiner	Signature	Date
_____	_____	_____
External Examiner	Signature	Date

ACKNOWLEGMENTS

I would like to convey my gratitude to my main supervisor Dr. Berhan Gessese for extending his generous support and patience as well as clarifying what I was thinking and contributing to the development of this research. He gave me constructive comments and critical reviews that make this study a success. His support and advice makes me motivated and energetic all the way through this study.

My endless gratitude is devoted to my beloved family. I sincerely thank my beloved family, especially my wife W/ro Hikel Ahmed Aboya who support me throughout the years. Thank you my wife for your endless care and love. You are all the reason for my success.

I wish to the special thank for W/ro Kides Alemu who introduced and detail information about the study area and give essential data about the research. I wish to thank my fellow graduate for sharing their proficiency and knowledge the intangible sources that actually went into producing this research.

I would like to express my gratitude to my office staff of landholding registration and information agency for permitting me to pursue this study. I also would like to thanks Addis Ababa University and the ministry of urban development and housing for granting the financial support for this research.

I am grateful to all organizations and individuals that contributed in my study. To begin with, many thanks go to staffs in GIS and surveying section of Hawassa city administration office and SNNP agriculture research office for genuinely offering their noble service in providing me data for this research. I also would like to thank National Meteorological Stations Agency (NMSA) for providing me data for this study.

Last but not least, I would like to extend my earnest thanks to my classmates, friends and colleagues who put a drop of contribution in any ways in my study.

ABSTRACT

The Hawassa Town was experienced a rapid urban expansion over the past two decades because of accelerated economic growth and increase in population which resulted in unplanned urbanization. Due to this, land use land cover change has been formed and will result environmental problems and challenges. To notice the above-mentioned problems, exploring the land use land cover dynamics which will finally resulted in the emergency of Urban Heat Island (UHI) will be assessed that will value` both the communities and local government in the cities. This research work was conducted on the relationship between land use transformation and its implication on land surface temperature change at the heart of rift valley, Hawassa Town, Ethiopia. Remote sensing, GIS techniques and statistical methods were mainly employed for data analysis. A series of Landsat data was used to assess and analyze urban landscape dynamics and land surface temperature. It does so by generating land use land cover maps derived from Landsat 5 TM for 1986, 1998 and 2010, and Landsat 8 OLI for 2017, using supervise classification techniques. Spatial pattern analysis of LST was performed using thermal band of landsat images. Cross tabulation methods, regression analysis and hotspot analysis was employed to study to urban landscape dynamics and land surface temperature. Based on the analysis done, it was obtained that the areal extant of urban (built-up) area has increased considerably by 121.68%.The increasing difference of Surface Heat Intensity (SHIn) between urban area and non-urban area was distinguished. For instance, non-urban area was cooler than the urban area except the agriculture sector. As per calculation performed, the difference of the mean of hotspot and mean of cold spot areas ranged from 8.8 °C to 14.37 °C. Therefore, increasing surface heat intensity was observed between 1986 and 2017. The surface temperature was found to be greater for agriculture and urban (built-up) land use land cover types. Finally, it has been concluded that, with rapid urbanization, surface thermal intensity increased but relationships with vegetation, water bodies and swampy area suggest that optional for mitigating urban warming in tropical climate may be available. The use of hotspot analysis and the investigations of the Urban Heat Island (UHI) will fill the research gaps for the rest of Ethiopian city for studies of urban thermal variations.

Key Word: Land use land cover, Land surface temperature, Urban Heat Intensity, Regression analysis, Cross Tabulation, Urban Heat Island.

Table of Contents

LIST OF TABLE

LIST OF FIGURE

LIST OF ABBREVATION

CSA	Central Statics Agency
ENVI	Environment for Visualizing Images
EMA	Ethiopia Meteorological Agency
EMR	Electro Magnetic Radiation
ERDAS	Earth Resources Data Analysis Systems
ESRI	Environmental Systems Research Institute
ETMs	Enhanced Thematic Mapper
DN	Digital Number
GIS	Geographical Information System
GPS	Global Positioning System
HLRIO	Hawassa Landholding Registration and Information Office
ITCZ	Inter Tropical Convergence Zone
LST	Land Surface Temperature
LULC	Land Use Land Cover
NDVI	Normalized Difference Vegetation Index
NDBI	Normalized Difference Built Up Index
NDWI	Normalized Difference Water Index
OLI	Operational Land Images (OLI)
RS	Remote Sensing
SHIn	Surface Heat Intensity
TIRS	Thermal Infrared Sensor
TM	Thematic Mapper
UHI	Urban Heat Island
UTM	Universal Transverse Mercator
USGS	United State Geological Survey
WWDSE	Water work design service enterprise

CHAPTER ONE

1. Introduction

1.1 Background of the study

Urbanization is a process whereby population move from rural to urban area and also from urban to urban area, enabling cities and towns to grow. It can also be termed as the progressive increase of the number of people living in towns and cities. It is highly influenced by the notion that cities and towns have achieved better economic, political and social mileages compared to the rural areas. Because of this cities and town are among the most complex land use structure crated by human societies. This complex system is characterized by the complex patterns of land use. In 2014 the world's urban population amounted to 54% of its total population. In the developed countries 78% of the population lived in urban areas, and in the developing countries, this figure was around 52%.this indicates that currently more than half of the world's population is urbanized (United Nations, 2014)[1].

Hawassa town was the most populated urban region in the country, which has been facing rapid urbanization over the decades. Factors responsible for rapid urban growth in the Hawassa town are physical conditions of the town, public service accessibility, employment opportunities, population growth, government plans and policies. By physical conditions, it means that the Hawassa town has topography suitable for the residence and the town near to Hawassa Lake.

Urban development usually gives to a dramatic change of the earth's surface as natural vegetation is removed and replaced by non-evaporating and non-transpiring surfaces such as metal, asphalt and concrete. This alteration will inevitably result in the redistribution of incoming solar radiation and induce the urban rural contrast in surface radiance and air temperature. Today, two-thirds of all impervious area is in the form of parking lots, driveways, roads, and Highways (Getter and Rowe, 2006). Therefore, high rate of urban landscape dynamics have resulted in radical demographic, economic, land use/land cover and climate changes. Climate changes are accompanying by the modern urbanization, especially in the case of rapid changes, where man has created his habitat (Kim, 1992).

Land Surface Temperature (LST) is an important parameter in the UHI phenomenon, which manifests high spatial and temporal in homogeneity especially in urban areas (Zaksek and Ostir, 2011). LST is actually the skin temperature of the land surface which differs from the land surface air temperature (Srivanit et al., 2012).

[1] (http://esa.un.org/unpd/wup/puplications/files/wup2004-report)

An Urban Heat Island (UHI) is an urban area which, significantly, warmer than its surrounding rural areas. The higher the urbanization, the larger temperature differences between urban and rural areas (S. Ahmed, 2017). Tall buildings and narrow streets can heat the air trapped between them, meanwhile, replacing natural land cover with concrete, infrastructure, and industrial activities take away the natural cooling effects (Weng and Larson, 2005). Increasing LST in urban areas leads to the formation of Urban Heat Islands (UHIs), where urban areas show higher LST than the surrounding rural areas (Buyantuyev and Wu, 2009).

So this research aims to investigate urban landscape dynamic and its impact on land surface temperature change in the study area. In this connection, satellite remote sensing provides a straight forward way to investigate the thermal differences between urban and rural areas, land use land cover change and retrieve land surface temperatures (LST). Land use/land cover change is strongly related to the urban growth, the study of the relationship between LST and land use/land cover is fundamental to explore the impact of urban growth on land surface temperature, including the UHI effect. The study of the relationship between LST and land use/land cover change helps researchers to understand the causes, spatial-temporal distributions, consequences and possible measures to mitigate the UHI effect.

The study on the UHI incident by satellite image derived by LST measurements is carried out by Landsat Thematic Mapper Sensor (TMs) and Enhanced Thematic Mapper Sensor Plus (ETMs+), particularly, have been utilized for local scale mapping studies of UHI (Weng and Qihao, 2012; Chen et al., 2002).The regression analysis and statistical measures are indeed useful to determine the influence degrees of LST within various land use/land cover types (Zhu and Zhang, 2011).

There are various types of land use/land cover indices proposed to investigate the correlations between land use/land cover and LST. Among several indices, Normalized Difference Vegetation Index(NDVI), Normalized Difference Built up Index (NDBI) and Normalized Difference Water Index(NDWI) strongly correlate with LST (Chen et al., 2006). These indices are extracted using band ratios of different bands of satellite images. Each of these indices has a unique spectral response to specific land use/land cover types (Guo et al., 2015).

The output of this research is assumed to fill this research gap through local scale analysis of landscape change detection and its influence on urban climate at a micro level and the existence of UHI phenomenon in the town. Exploring the impact of urban growth on LST can be useful for the urban planners and decision makers for sustainable urban planning and to discover ways to solve the urban environment problems.

1.2 Statement of the problem

Urban landscape dynamics mainly depends upon the city requirement, facilities available and industrialization. Due to this, accelerated economic development and population of the town increase over the years. The major causes of migration of the people from rural to urban areas, putting huge pressure on infrastructure, nature resource and lead to formation of slums or uncontrolled urban expansion. Because of the increasing of population, industrialization and other natural and human activities, its land use land cover patterns are changing. This numerous changes in the land use land cover patterns increment in urban expansion. Finally, increases level of urban expansion which in turn increases the pressure on environment change.

In the recent time, global warming and environmental problems are a headache for both developing and developed countries. Global climate appears to be changing at an alarming rate (Naissan and Lily, 2016). Both urban and rural areas are experiencing warm temperature condition and it is increasing from time to time. The earth's environment is a dynamic system, including many interacting components (physical, chemical, biological and human) that are continuously varying (Emilio, 2008). Therefore, the climate change was one of the most influential physical factors that not only impact individual's psychology and physiology but also control the life of behavioral and economical activates. The climate still affects the comfort of the personal indoors and outdoors (Anbar, 2012).

Practices such as changing the land use land cover of agriculture land and vegetation cover changed into industry, residence and unplanned settlement and other activities lead our environment changed into warming the temperature. Accordingly, one of the main factors, that is responsible for the increment of environmental change especially land surface temperature change is land use land cover change. As surfaces throughout the entire city become hotter, overall ambient air temperature increases. There is a rise in air pollution and heat, which has various level of harmful on the population.

This study tries to show a wide array of applications that gives information about the correlation between LST and land use land cover dynamics process of the area as an input for planning and decision-making.

1.3 Objective of the study

1.3.1 General objective

- The general objective of this study was to assess urban landscape dynamics and its implication on land surface temperature change through GIS and remote sensing techniques in Hawassa Town and its surroundings area.

1.3.2 Specific objective

- To quantifying the magnitude of urban landscape dynamics since 1986.
- Investigate the relationships between land surface temperature and land use land cover indices and land use land cover types; and
- Analyze Surface Heat Intensities (SHIn) and examine its temporal and spatial variation across Hawassa Town and its surroundings.

1.4 Research questions

The study will address the following research questions.

For Objective 1

- What are the spatiotemporal patterns of land use land cover changes of the study area?
- How accurate the land use land cover map as derived from image classification?
- What are the major land use land cover classes of the study area?

For Objective 2

- What is the role of NDVI, NDBI and NDWI for land surface temperature analysis?
- What is the correlation between land use land cover indices and LST in the study area?
- What is the impact of each land use land cover types on LST change in the study area?

For objective 3

- How is the spatial-temporal pattern, trends and distributions of land surface temperature in the study area?
- What are the surface heat intensity and its spatio-temporal pattern?

1.5 Scope of the study

The present study was conducted in and around Hawassa Town in SNNP Region; Ethiopia. The study areas have different land use land cover patterns and the different land use land covers have been changing from time to time. Because of the land use land cover change, the LST of Hawassa Town and its surroundings has been rising from time to time. Increasing LST leads to environmental problem such as climate change and seasonal fluctuation. However, the increase of LST is not supported by research rather than the perception of local communities.

In order to know and compute the implication of the urban landscape dynamics on land surface temperature change, correlation analysis between the land use/land cover and LST was done. For each land use/land cover classes the LST values assessed by zonal statistic tool and land use/land cover classification should be supported by field verification and high resolution image. Unless land for settlements and farm land properly managed, it can affect and have a negative impact on the environment. Therefore, to overcome this problem, the present study would contribute for decision makers as information and identifying different land use/land cover classes and changes.

1.6 Significance of the study

The significance of the study could be, 1) give information about the trend of land use/land cover and LST Change of the area; 2) give the information about the Surface Heat Intensity in the temporal resolution in the study area; 3) It could be used as an input for government policy makers, urban and rural land management, natural resources managers, environmental experts and other concerned bodies for their decision making processes related to how land use/land cover and LST changes through time. In addition to this, it can be a reference or initial step and use as input for coming researchers based on the analysis of the study. In addition, it helps to quantify the relationship between land use/land cover types and land use/land cover indices with LST, and can be an important input to predict future land surface warming.

The output of the study would provide better information about the changes in urban areas and surrounding area by using the application of GIS and remote sensing techniques or geospatial tools and its applicability, which is time and cost effective for analysis and impact of land use land cover dynamics on LST. It also provides the opportunity to understand the trends of changes and its driving factors.

1.7. Limitations of the study

Despite the fact that Hawassa Town is one of the fastest growing town in Ethiopia but its implication on surface urban heat island it is rather less studied in comprehensive analyze urban landscape dynamics and its effect on urban heat island and the published literature not obtained from the international published site and in addition to this for urban researcher those important document like aerial photo and other reference data for accuracy assessment in digital format are inaccessible both in the regional as well as in the federal urban development office. And also, not obtain the complete monthly record temperature data from 1986 to 2017 and the meteorological station data not cover the whole study area because of this not validate of land surface temperature obtained from Landsat thermal bands. During the processing and analyzing of an overall input dataset there have been some limitations encountered by the researcher. That includes: Time was a very critical problem to cover all the activities. Financial resources limitations to cover all the necessary required expense for technical assistant and material supply.

1.8 Thesis structure

The present work has been organized in six chapter and the outline of each chapter is mentioned below. Chapter one presents the introduction and explains background of the study and justification of the study, research problem, significance, scope of the study, research objective and research questions. Chapter two is the Literature review part reviews the concepts that are related to the land use/land cover and urban climate change. And also, Describe about GIS and Remote sensing techniques, the role of GIS and remote sensing for LULC and LST change analysis and the parameter for calculate land surface temperature. And finally, describe the land use land cover indices and impact of LULC on LST change. Chapter three presents the study area description such as location and accessibility, climate, physiographic population and wind of the study area. Chapter four describes data source and research methods that were applied and developed. Chapter five presents result and discussion of the thesis. It starts spatial distribution of land use land cover, change detection of the land use/land cover and the relationship between LST and land use land cover. Chapter six summarizing and concludes the finding in the thesis and gives an outlook on future research in the field.

CHAPTER TWO

2. Literature review

2.1 The concept of land use land cover

Every parcel of land on the Earth's surface was unique in the cover it possesses. The earth's surface has been changed considerably in the past decades by human's as a result human induced factors of deforestation, agricultural activities and urbanization. Land is the ultimate resource of the biosphere. Land use and land cover are distinct yet closely linked characteristics of the Earth's surface. The definition land use and land cover has been used as one in different research. However, these two terms explain two different issues and have different meanings.

Land-cover refers to the observed biophysical cover on the earth's surface, including water bodies, vegetation, soil and hard surfaces (FAO, 2000).**Land-use** is the exploitation/utilization of the land by human activities for the purpose of settlements, agriculture, forestry, and by pasture altering land surface processes including bio geochemistry, hydrology and biodiversity (Di Gregorio and Jansen, 2000). In this context, as variation in the surface component of the landscape and is only considered to occur if the surface has a different appearance when viewed on at least two successive occasions (Lemlem, 2007).

2.2 Drivers of land use land cover change

Many researchers agrees that the main cause of land use land cover change and related impacts in Ethiopia are anthropogenic in origin even though natural processes may also contribute to change (Agarwal *et al.*, 2002;Ali, 2009 and Birhan and Assefa, 2017). Changes in the land use land cover reflect the history and, perhaps, the future of humankind. Such changes are influenced by a variety of factors related to human population growth, economic development, technology and environmental changes (Houghton, 1994). Population growth is one of the major factors for land use land cover change. People are the most important natural resources, which is mutually inter-related and interdependent for their sustainable development (Santa, 2011).

Land-cover changes, which is conversion of the land-cover from one type of to another and modification of the conditions within a category and land-use change occurs initially at the level of land parcels when land managers decide that a change towards another land utilization type is desirable (Meyer and Turner, 1992).

United States Environmental Protection Agency (USEPA, 2004), identified that the major drivers of Land-use/Land-cover change are:

- Natural process such as climate and atmospheric changes, wildfire and past infestation.
- Direct effect of human activity such as road and illegal house constructions and deforestations (Clearance of trees).
- Indirect effects of human activity is such as, water diversion leading to lowering of the water table.

The other factors that contributed to the Land-use/Land-cover change are property rights. Private ownership protected forests to some extent during the imperial reign (Adugna et al., 1996). Land degradation is the most series impact of land-use/land-cover changes happened in Ethiopia. land degradation, which is decreasing of potential of productivity of land is caused by different processes including soil erosion and nutrient depletion and so on These processes are interrelated and could occur due to natural drivers but they are invariably accelerated by human intervention in the natural environment(Agray-Menash,(1985).

2.3 The concept of urban climate change

Climate change, broadly speaking, refers to any significant change in measures of climate such as temperature, precipitation, or wind lasting for an extended period decade or longer. And also climate change refers to long term or permanent shift in climate of the urban area. Some of the evidence for climate change includes increased frequency of the occurrence of drought, global temperature rise, tropical cyclones, flood, and reduced annual rainfall reduction in glacial cover over mountain and rising sea levels (Alemayehu, 2008). The term climate change is often used interchangeably with the global warming, but according to the National Academy of Sciences (2008 Edition), the phrase climate change 'is growing in prefer used to 'global warming' because it helps convey that there are changes in addition to rising temperature.

The climate in urban areas differs from that in neighboring rural areas, as a result of urban development. Urbanization greatly changes the form of landscape, and also produces changes in an area's air. Urban climate, any set of climatic conditions that prevails in large metropolitan area and that differs from the climate of its rural surroundings. Urban climates are distinguished from those of less built-up areas by differences of air temperature, humidity, wind speed and direction, and amount of precipitation. These differences are attributable in large part to the altering of the natural terrain through the construction of

artificial structures and surfaces. For example, tall buildings, paved streets, and parking lots affect wind flow, precipitation runoff, and the energy balance of a locale.

2.4 Remote sensing

Remote Sensing is the science and art of acquiring information about material objects, area, or phenomenon, without any physical contact between the object and sensors. In remote sensing, information transfer is accomplished by use of electromagnetic radiation (Lillesand and Kiefer, 2004).

Image processing and analysis can be defined as the "act of examining images for the purpose of identifying objects and judging their significance". Image analyst study the remotely sensed data and attempt through logical process in detecting, identifying, classifying, measuring and evaluating the significance of physical and cultural objects, their patterns and spatial relationships1[2].

Digital image consists of discrete picture elements called pixels. Associated with each pixel is a number represented as DN (Digital Number) that depicts the average radiance relatively small area with in a scene. The range of DN values being normally 0 to 255. The size of this area affects the reproduction of details within the scene. As the pixel size is reduced more scene detail is preserved in digital representation (Lillesand and Kiefer, 2004). Digital image analysis is usually conducted using raster data structure-each image is treated as an array of values. It offers advantages for manipulation of pixel values by image processing system, as it is easy to find and locate pixels and their values.

2.4.1 Resolution

Resolution is an important term commonly used to describe remotely sensed imagery. There are four distinct types of resolution. These are spatial, spectral, radiometric, and temporal. These resolution characteristics help to describe the functionality of both remote sensing sensors and remotely sensed data (ERDAS Field Guide, 2002).

Spatial resolution is the measure of the smallest object that can be resolved by the sensor or the smallest area on the ground represented by each pixel. It tells the degree of detail of the earth surface feature recorded by the sensor. The finer the spatial resolution in remote sensing refers to imagery in which each pixel represents a small area on the ground and the detail the recorder. Small scale refers to imagery in which each pixel represents a large area on the ground.

[2](http://www.ida.liu.se>Literature>image processing and analysis)

Spectral resolution refers to the specific wave length intervals in EM spectrum sensor can record. Wide intervals in the electromagnetic spectrum are referred to as coarse spectral resolution, and narrow intervals are referred to as fine spectral resolution.

Radiometric resolution refers to the dynamic range, or number of possible data files value in each band. This is referred to by the number of bits into which the recorded energy is divided. The total intensity of the energy, from 0 to the maximum amount, the sensor measures is broken down, for example, into 256 brightness values for 8-bit data. The data file values range from 0, for no energy return, to 255, for maximum return, for each pixel.

Temporal resolution is a measure of how often a given sensor system obtains imagery of a particular area, or how often an area can be revisited or the frequency at which satellite data is recorded about an earth surface feature. Temporal resolution is an important factor to consider in change detection studies.

2.4.2 Image processing

Image processing is a mathematical manipulation and interpretation applied on the pixel value and/or its geometry. Is broadly classified in to preprocessing and post-processing. Pre-processing operations, which are also called image restoration and rectification, are essential for prior to image classification and change detection analysis. It involves correction of sensor- and platform-specific radiometric and geometric distortions of data.

Radiometric corrections removes errors related with variation of illumination and viewing geometry, atmospheric conditions, and sensor noise and response. Radiometric preprocessing influences the brightness values of an image to correct for sensor malfunction or to adjust the value to compensate for atmospheric degradation. Absolute radiometric calibration techniques require ground reflectance data and information about the sensor and atmosphere for the date of image acquisition, which are often difficult or impossible to obtain. William et al. (1997) the atmosphere degrades the true DN value of earth feature by introducing additional brightness from its components by scattering. The preprocessing operation to correct atmospheric degradation; haze correction or dark subtract, is used to compensate this error.

Geometric distortions can be caused by several factors, including: the perspective of the sensor optics; the motion of the scanning system; the motion of the platform; the platform altitude and velocity; the terrain relief; and, the curvature and rotation of the Earth. The sources of geometric distortions are classified in two categories: Observer and Observed. Geometric corrections are intended to compensate for these distortions so that the geometric

representation of the imagery will be as close as possible to the real world (Chintan P. Dave, 2015).

Image enhancement: is basically improving the interpretability or perception of information in images for human viewers and providing `better' input for other automated image processing techniques. The principal objective of image enhancement is to modify attributes of an image to make it more suitable for a given task and a specific observer. During this process, one or more attributes of the image are modified. The choice of attributes and the way they are modified are specific to a given task. Moreover, observer-specific factors, such as the human visual system and the observer's experience, will introduce a great deal of subjectivity into the choice of image enhancement methods. There exist many techniques that can enhance a digital image without spoiling it. The enhancement methods can broadly be divided in to two such as spatial domain methods and frequency domain methods (Raman Maini and Himanshu Aggarwal, 2010).

2.5 Geographical Information System (GIS)

Geographic Information Systems is a computer based system that provides four sets of capabilities to geo-referenced data: data input, data management (storage and retrieval), manipulation and analysis, and finally data output (Arnoff, 1989).GIS is a set of tools for collecting, storing, retrieving at will, transforming and displaying spatial data from the real world for a particular set of purposes (Burrough, 1986). Furthermore, a Geographic Information Systems is a computer based system which is used to digitally reproduce and analyze the future at present on earth surface and the events that take place on it.

In order to utilize the land resources in sustainable way, a land use plan that incorporates the different land characteristics has a paramount importance. To incorporate the different land attributes that differ spatially and to identify the best suitable land use, GIS is a vital tool. Geographic Information Systems (GIS) incorporates database systems for spatial data. Moreover, the surface and overlay analysis capabilities in GIS can effectively facilitate in handling vast amount of spatial information (Dayawansa, 2003).

It is estimated that 80% of data used by managers and decision makers is related geographically. Data are of little value in and of themselves. To be useful, they must be transformed in to information. When data are organized, presented, analyzed, interpreted, and considered useful for the decision problem, they become information. Accordingly, geographical information can be defined as georeferenced data that has been processed in to a form that is meaningful to the recipient (decision makers) and it is of real or perceived value

in the decision-making process. Information is used by the decision maker and is derived from data (Malczewski 1999).

2.6 The role of remote sensing and GIS for LULC and LST change analysis

Remote sensing and geographic information system techniques have been widely used over the world for the study of historical changes in land use and land cover and Land surface temperature analysis. Remote sensing has been used to identify vegetation cover, air pollution, LST and other surface characteristics (Zha, 2012; Weng, 2004). Furthermore, understanding the correlation between land surface temperature and land use land cover is important to manage the land. It provides a large variety and amount of data about the earth's surface for detailed analysis as well as change detection quantification using ground borne, airborne and space borne derived datasets with the availability of historical remote sensing data, the reduction in data cost and increased resolution from satellite platforms, remote sensing technology appears ready to make an even greater impact on monitoring land-cover change. Land-use/land-cover changes can be analyzed over a period using Landsat sensors such as Landsat Multi Scanner (MSS) data and Landsat Thematic Mapper (TM) data by image classification techniques (Gumindoga, 2010).

Since 1972, Landsat satellites have provided repetitive, synoptic, global coverage of high-resolution multispectral imageries. Their long history and reliability have made them a popular source for documenting changes in land use/land cover over time(Turner *et al.*, 2003) and their evolution is further marked by the launch of Landsat7 (Enhanced Thematic Mapper Plus sensors) by the United State in 1999.

According to Macleod and Congation (1998), the following are four land use land cover change detection (aspects of change detection) are distinguishing the nature of the change; detection/finding of the changes that have occurred; measuring the area extent of the change and assessing and investigating spatial pattern of the change.

Remote Sensing and geospatial tools play crucial role in quantifying and estimating LST. Land surface temperature is derived from geometrically and radiometric corrected Landsat Thermal Infrared (TIR) band 6 and Landsat 8 thermal infrared (TIR) band 10 and 11(Khin *et al.*, 2012).

2.7 Land surface temperature driving from remotely sensed data

2.7.1 Sensor brightness temperature

The brightness temperature is a measurement of the radiance of the microwave radiation traveling upward from the top of the atmosphere to the satellite, expressed in units of the temperature of an equivalent black body. The brightness temperatures, measured at different microwave frequencies, are used at remote sensing systems to derive wind, vapor, cloud, rain, and sea surface temperature products. Despite differences in sensor frequencies, channel resolutions, instrument operation and other radiometer characteristics, RSS produces high-quality, carefully inter calibrated data, using uniform processing techniques, with a brightness temperature data record spanning multiple instruments over several decades.

2.7.2 Land surface emissivity

Surface emissivity (ε) is a measure of the inherent efficiency of the surface in converting heat energy into radiant energy above the surface. It depends on the composition, roughness, and moisture content of the surface and on the observation condition (i.e. wavelength, pixel resolution and observation angle(J.A. Sobrino, Raissouni and Zhao-Liang Li, 2001).Accurate surface emissivity is desired in land surface models for better simulations of surface energy budgets from which surface temperature in the model is calculated (Jin et al. 1997).Emissivity (ε) is defined as the "emitting ability" of a natural material, compared to that of an ideal blackbody at the same temperature. The emissivity of natural land surface is determined by soil structure, soil composition, organic matter, moisture content, and vegetation-cover characteristics (Van de Griend and Owe, 1993) the value of the emissivity always lies between 0 and (Jin and Liang, 2006) .

The value of emissivity always lies between 0 and 1 (Jin and Liang, 2006). The knowledge of surface emissivity is important for estimating the land surface temperature. It can reduce the error on estimating the surface temperature from thermal satellite data. Current emissivity databases consists MODIS, ASTER and Landsat products.

Emissivity has strong seasonality and land use/land cover dependence. Specifically, emissivity depends on surface-cover type, soil moisture content, soil organic content, vegetation density. For example, broadband emissivity is usually around 0.96–0.98 for densely vegetated areas, but it can be lower than 0.90 for bare soils (Jin and Liang, 2006).

Land Surface Emissivity (LSE), as an intrinsic property of natural materials, is often regarded as an indicator of material composition, especially for the silicate minerals, although it varies with viewing angle and surface roughness (Sobrino, Raissouni and Li 2001; Sobrino, Jimenez-Munoz and Verhoef, 2005).

Generally speaking, the retrieval of LSE from space is not easy. The direct estimation of LSE from passive satellite measurements is impossible due to the combined effects of the land surface temperature (LST) and LSE or the atmospheric contamination (Li, Petitcolin, and Zhang 2000; Jiang, Li, and Nerry 2006).

2.7.3 Land surface temperature

Land surface temperature denotes the temperature on the surface of the earth or it is the skin temperature of the earth surface phenomena (Kayet *et al.*, 2016).Land Surface Temperature (LST) is the radiative skin temperature of the land derived from solar radiation that is a measurement of how hot the land is to the touch. Skin temperature refers to the temperature of the top surface in bare soil conditions and to the effective emitting temperature of vegetation "canopies" as determined from a view of the top of a canopy (esa, sentinel online)[3].A simplified definition would be how hot the "surface" of the Earth would feel in a particular location. From a satellite's point of view, the "surface" is whatever it sees when it looks through the atmosphere to the ground. It could be snow and ice, the grass on a lawn, the roof of a building or the leaves in the canopy of a forest. Land surface temperature is not the same as the air temperature that is included in the daily weather report because land heats and cools more quickly than air. But average monthly land surface temperature in degrees Celsius as measured by the Moderate Resolution Imaging Spectro Radiometer (MODIS) on NASA's terra satellite. LST is the brightness temperature of land surface; it's not the real temperature on the surface but has strong relationship with air temperature[4]. Thus, LST could be an indicator for UHI. Land surface temperature is important for evaluating land surface and land atmosphere interaction, constraining surface energy budgets and model parameters and providing observation of surface temperature change both globally and key regions.

LST is a basic determinant of the terrestrial thermal behavior, as it controls the effective radiating temperature of the Earth's surface. However, because of the extreme heterogeneity of most natural land surface, this parameter is difficult to estimate and validate. Several factors can fundamentally influence the derivation of LST including temperature variations

[3]https://sentinel.esa.int/web/sentinel/user-guides/sentinel-3-slstr/overview/geophysical-measurements/land-surface-temperature)

[4]https://www.researchgate.net/post/What_is_the_difference_between_Land_Surface_Temperature_LST_and_Urban_Heat_Island_UHI)

with angles sub-pixel in-homogeneities in temperature and cover, surface spectral emissivity at the channel wavelengths, atmospheric temperature and humidity variations and clouds and large aerosol particles such as dust.

Land surface temperature of a given area can be determined based on its brightness temperature and the land surface emissivity, which is calculated through applying the split window algorithm (Rajeshwari and Mani, 2014, MdShahid, 2014). According to Kerr *et al.* (2004) land surface temperature gives information about the difference of the surface equilibrium state and vigorous/vital for many applications. LST also defined as, the monitoring of surface temperature based on pixel derived observation through remote sensing (Paramasivam, 2016). The characteristics of urban land surface temperature is depending up on its surface energy balance, which is governed by its properties such as orientation, sky and wind, openness to the sun and radiative ability to reflect solar and infrared and also ability to emit infrared availability of surface moisture to evaporate and roughness of the surface (Voogt,2000). Land-use/land-cover changes due to changes in surface temperature (ST) which makes both urban and rural managers to estimate the urban surface temperature and its surrounding rural area for urban planning as well land management in general (Becker *et al.*, 1990).The LSI of a place is the indicator of its climate change and radiation exchange with atmosphere. It is important for meteorology, soil moisture and environmental studies.

2.8 Urban Heat Island (UHI)

Urban Heat Island (UHI) is an urban or metropolitan area that is significantly warmer than its surrounding rural areas due to human activities. The term heat island describes built up areas that are hotter than nearby rural areas (Sobrino *et al.*, 2012). Generally, Urban Heat Island (UHI) is a specific area, generally in urban regions where the environment is much hotter than the nearby rural areas because of human activities. The heat is most prominent in night times and during cloudy conditions. It affects the local climate and public health and consumes more energy for air-conditioning or refrigeration. It is not a direct indication of global warming. Urban development reduces vegetative cover and adds heat absorbing surface such as a roof tops, building and paving. Heat is also added from other source in cities such as fuel combustion and air conditioning unites. The results are an urban heat island. Experts often divide the urban heat island into three types: atmospheric (surface), canopy, and boundary layer Surface heat islands.

Atmospheric heat islands- Warmer air in urban areas compared with rural areas, illustrated with isotherm maps or graphs.

Canopy layer heat islands are present in the air layer where we live-from ground level to the tops of tree or buildings.

Boundary layer urban heat islands-start from the rooftop and treetop level and extend up to the point where urban landscapes no longer influence the atmosphere. This region typically extends no more than one mile (1.5 km) from the surface.

2.9 Land use land cover indices

2.9.1 Normalized Difference Vegetation Index (NDVI)

Normalized Difference Vegetation Index is the difference of near infrared and visible red reflectance values normalized over reflectance and calculated from reflectance measurements in the near infrared (NIR) and red portion of the spectrum (Burgan and Hartford, 1993). To calculate the Normalized Difference Vegetation Index, subtracting the red band from near infrared band and then dividing to near infrared band plus red band. The value is ranging from -1 to1, the negative values are indicative of water, snow, clouds, non-reflective surface and other non-vegetated, while the positive value expresses reflective surfaces such as vegetated area (Burgan and Hartford 1993). Vegetation has a direct match/correspondence with thermal, moisture and radiative properties of the earth's surface that determine LST (Weng, 2004). In addition to NDVI, Normalized Difference Moisture Index (NDMI) also used as an alternative indicator of surface urban heat island effects in Landsat imagery by investigating the relationships between land surface temperature and NDVI. The index is expressed as NDMI= (NIR-IR)/ (NIR+IR), it evaluates the different content of humidity from the landscape elements, especially in soils, rocks and vegetation and it is an excellent indicator of dryness. Values greater than 0.1 are symbolized light colors and they signal high humidity level. Whereas, values close to -1 symbolized by dark colors represents low-level humidity level (Mihai, 2012).

According to streutker (2003), one of the promising of studying urban surface temperature is using remote sensing or air born technology. Evaluation of land surface temperature from remotely sensed data is common and typically used in studies of evapotranspiration and desertification processes.

Further, (Walsh *et al*., 2011) stated that urban area such as buildings and roads and infrastructures or anthropogenic factors contribute to increase atmospheric temperature. The wide use of land surface temperature for environmental studies, have made remote sensing of land surface temperature important academic issue during the last decades. Indeed, one of the most important parameters in all surface atmosphere interactions and fluxes between the land

and the atmospheric island surface temperature (Buyadi *et al*, 2013).NDVI use Landsat 5 TM the reflectance in the Near-infrared band (0.76-0.9µm) and red band (0.63-0.69µm) and for Landsat 8 OLI Near-infrared band (0.85-0.88µm) and red band (0.64-0.67µm).

Mathematically, NDVI were calculated using the following formula:

$$\mathrm{NDVI} = \frac{\mathrm{NIR} - \mathrm{R}}{\mathrm{NIR} + \mathrm{R}} \qquad (2.1)$$

Where: NDVI-Normalized Difference Vegetation Index,

NIR-Near-Infrared and,

R- Red Band

2.9.2 Normalized Difference Built-up Index (NDBI)

NDBI was first developed by (Zha, Y., Gao, J. and Ni, S., 2003) to investigate the extent and density of imperviousness surface and built-up area sand map these areas, as it can highlight the urban distribution with a typically higher reflectance in the short-wave infrared region band than that of the near-infrared one (Alhawiti, R.H. and Mitsova, D., 2016).The NDBI separates Built-up from other ground cover. Its ratio was calculated through the difference of Short-wave Infrared Band (SWIR) and near infra-red (NIR) which was normalized by summing up these two bands. NDBI use NIR and SWIR are the reflectance in the Near-Infrared band (0.76 -0.9 µm) and Short-wave Infrared band (1.55 - 1.75 µm), respectively, for Landsat 5 TM. However, for Landsat 8 OLI these differed slightly: Near-Infrared band (0.85 - 0.88 µm) and Short-wave Infrared band (1.57 - 1.65 µm)

Mathematically NDBI were calculated using the following formula:

$$\mathrm{NDBI} = \frac{\mathrm{SWIR}-\mathrm{NIR}}{\mathrm{SWIR}+\mathrm{NIR}} \qquad (2.2)$$

Where: NDBI-Normalized Difference Built-up Index

SWIR-Short-wave Infrared Band

NIR- Near-Infrared Band

2.9.3 Normalized Difference Water Index (NDWI)

NDWI is an index to extract water bodies from satellite imagery. The value is same here for the reason of being NDWI indices value from -1 to 1. NDWI has been developed to delineate open water and enhanced their presence in remote sensed imagery based on reflected near infrared radiation and visible green light. NDWI may allow turbidity of water bodies to be estimated from remote sensed data (McFeeter, 1996). NDWI is sensitive to change in liquid water content of vegetation canopies. Water has a high reflectance in the Short Wave Infrared

Red (SWIR) and Green band bands of a sensor system. The NDWI separates water from other water cover. Its ratio was calculated through the difference of Green (G) and Short-wave Infrared Red (SWIR) which was normalized by summing up these two bands. NDWI use Green and SWIR are the reflectance in the Green band (0.52 - 0.60 µm) and Short-wave Infrared band (1.55 - 1.75 µm), respectively, for Landsat 5 TM. However, for Landsat 8 OLI these differed slightly: Near-Infrared band (0.85 - 0.88 µm) and Short-wave Infrared band (1.57 - 1.65 µm).

$$\text{NDWI} = \frac{\text{G}-\text{MIR}}{\text{G}+\text{MIR}} \qquad (2.3)$$

Where: NDWI-Normalized Difference Water Index,

G-Green and,

SWIR-Short-wave Infrared Band

2.10 Impact of LULC change on land surface temperature change

One of the major factors that are responsible for the increase of land surface temperature is land use/land cover and different researchers agree with that land-use change and unplanned use of land resources lead to increasing land surface temperature. (Oluseyi *et al.*, 2011) have studied that spatially there are correlations with changes as reflected in the characteristics of individual land-use classes or categories. The influence of land use/land cover changes on LST is different at different latitude, for example in South Asia and East Asia tropical temperate regions (Shukla, 1990).

According to Yue *et al.* (2007), the relationship between NDVI and LST with integrated remote sensing application to quantify Shanghai Landsat7 ETM+ data was used. The result shows that different land use/land cover classes have significantly different impacts on land surface temperature and normalized difference vegetation index calculated by the Enhanced Thematic Mapper Plus sensor in the Shanghai urban environment.

CHAPTER THREE

3. Description of the study area

3.1 Location and accessibility

This study area was carried out in Hawassa town and surrounding area. It is located in the southern Nations, Nationalities and peoples (SNNP) regional state. It is a city in Ethiopia, on the shores of lack Hawassa in Great Rift Valley. It is found at the distance of 273 km south of Addis Ababa via Bishoftu, 130km east of Sodo and 75km north of Dilla. One of the most rapidly expand city in the country. It is located a latitude and longitude of $6^0$96'N $38^0$21'E and $7.14^0$96'N $38^0$36'E in geographical coordinate Systems. The city administration has an area of 157.2 Square km, but the overall study area has an area of 560 square Km.

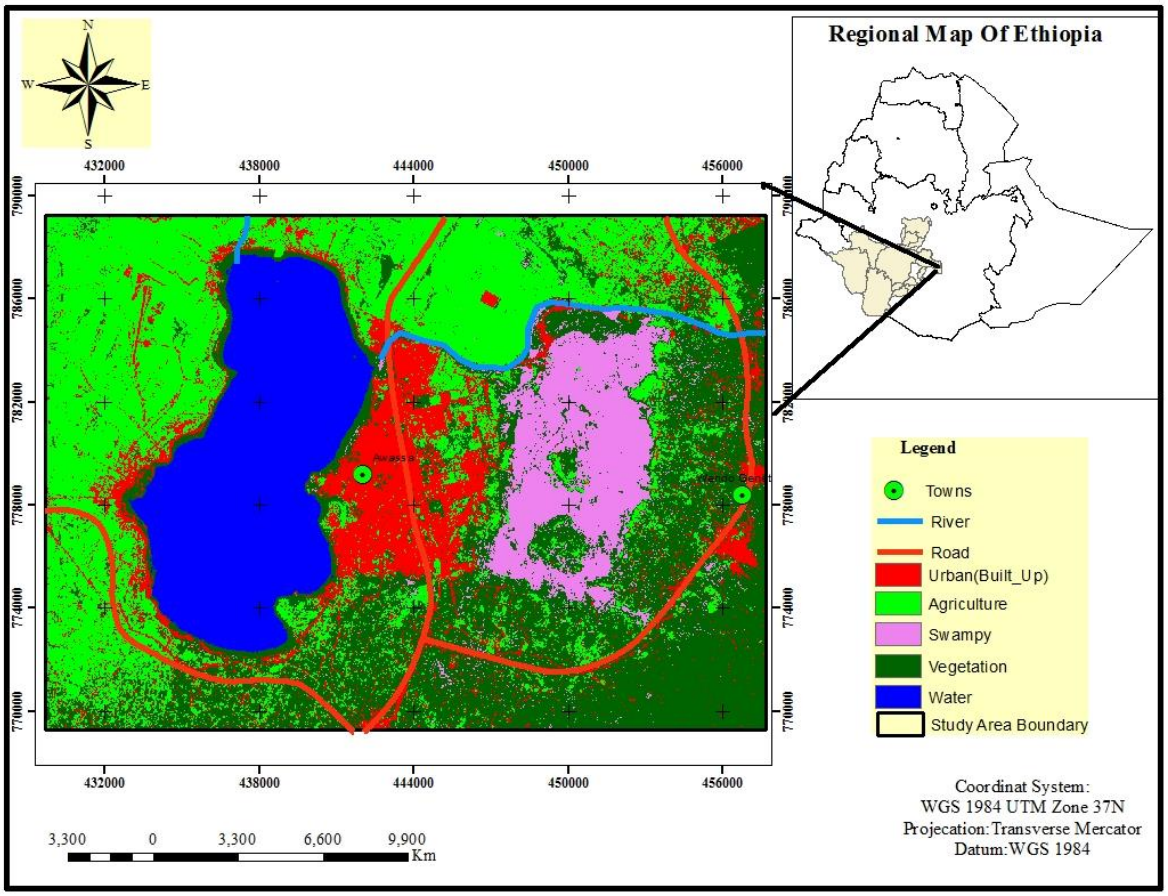

Figure 3.1: Location map of the study area.

3.2 Climate

Hawassa has a tropical savanna climate though it boarder on a subtropical highland climate. There are two seasons: a length thought not intense wet season from March to October and a short dry season from November to February. The extra cloudiness of the wet season was sufficient to make it substantially cooler than the dry season despite a higher sun angle. However, the coolest morning temperatures, often close to freezing, occur during the dry season.

3.2.1 Rainfall

Ethiopia is located in the region where June through September the main rainy season. The moisture for precipitation in the area originates from southwest equatorial air stream, which moves northwards with inter-tropical convergence zone (ITCZ), (W.W.D.S.E 2001). The mean annual rainfall computed from the long-term (1985 to 2017) on the bases of 32 years of the record of one rainfall stations in Hawassa meteorological station that contribute to the study area was estimated to be 973mm. Kiremet (June to September) rainfall contribute 48%, Baga (October to February) rainfall contribute 20% and Belg season (March to May) rainfall contribute 32% to the mean annual precipitation in the Hawassa town (Figure 3.2). shows the long-term average monthly distribution of rainfall at Hawassa meteorological station and the an average of 973mm rain fall par year.

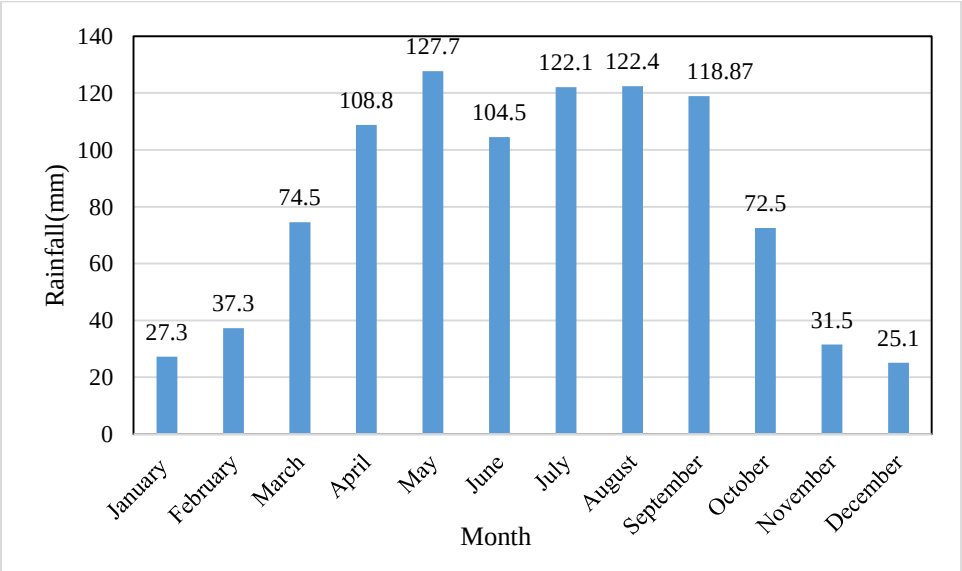

Figure 3.2: Monthly average rainfall for Hawassa and surrounding area at Hawassa meteorological station (1985 - 2017).

3.2.2 Temperature

The mean annual temperature computed from the long-term (1985 to 2017) on the bases of 32 years of the record of one temperature stations in Hawassa meteorological station that contribute to the study area was estimated to be 27.45^{0}C in maximum temperature,13.04^{0}C in minimum temperature and 20.25^{0}C the mean temperature. The monthly average maximum temperature of the area varies from 24.57^{0}C to 29.99^{0}C, the monthly average minimum temperature of the area varies from 10.36^{0}C to 14.58^{0}C and the monthly average mean temperature of the area varies from 19.32^{0}C to 21.57^{0}C.The absolute maximum temperature occurs in mid-March and is 29.99^{0}C and the absolute minimum temperature occurs in December and is 10.36^{0}C(Figure 3.3).Variation of monthly average temperature in Hawassa (1985-2017) adapted from National Meteorological Agency (NMA) of Ethiopia, 2017.

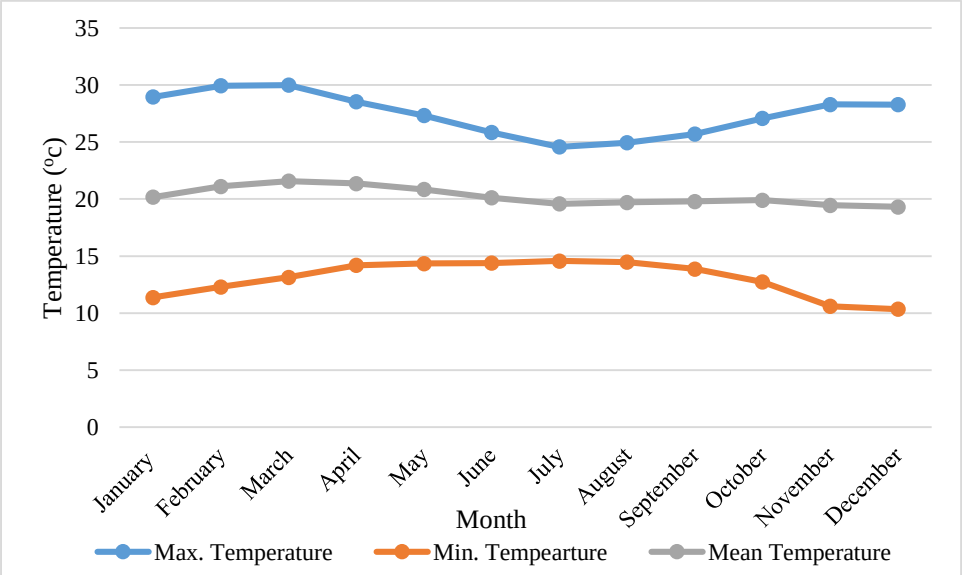

Figure 3.3: Monthly average temperature for Hawassa and surrounding area at Hawassa meteorological station (1985 - 2017).

3.2.3 Relative humidity

We base the humidity comfort level on the dew point, as it determines whether perspiration will evaporate from the skin, thereby cooling the body. Lower dew points feel drier and higher dew points feel more humid. Unlike temperature, which typically varies significantly between night and day, dew point tends to change more slowly, so while the temperature may drop at night, a muggy day is typically followed by a muggy night. The perceived humidity level in Hawassa, as measured by the percentage of time in which the humidity comfort level

is muggy, oppressive, or miserable, does not vary significantly over the course of the year. At a station in Hawassa town RH has been measured three times a day, since 1985. The Relative humidity records show the mean monthly value of 66.48% with mean minimum monthly of 57.15% in February and reaches maximum 76.13% in September. Long-term mean monthly values of climatic variables are presented in the following (Figure 3.4).

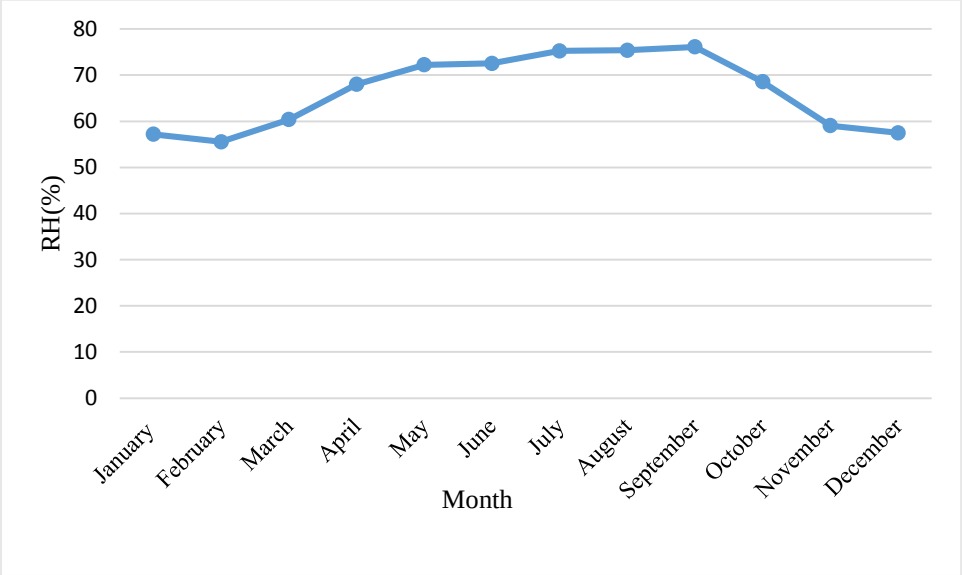

Figure 3.4: Monthly average relative humidity for Hawassa and surrounding area at Hawassa meteorological station (1985 - 2017).

3.3 Physiographic and drainage

The study area, Hawassa town and its surrounding is situated in a large volcano-tectonic collapse (Hawassa caldera) at the eastern margin of the MER, having a diameter of 40-50Km, (Woldegabriel et al., 1986). The study area was characterized by flat lying topography with some scattered hills, like Mount Tabor (1800m), Mount Alamura (2019m).Therefore, the average altitude of the city is 1708m (5604 ft.).The depression is bounded by remnants of the caldera wall and some regional and local faults. The eastern scarp forms the edge of the rift whose average throw is about 500 m, whereas the southern and western scarps of the caldera which roughly form an arc of a circle are relatively lower with a 250 m elevation difference from the floor. Lake Hawassa was a closed catchment with no surface water out flow. It is fed by some ephemeral streams from the west and North West and by Tikurwuha River from the east, which is the only perennial river that flows to the lake. The former Lake Cheleleka is converted to swamp since sediments that are coming from the eastern side of the scarp are partly deposited in this area.

3.4 Population

Based on the 2007 census conducted by the Central Statistical Agency of Ethiopia this town has total population of 157,139 out of this 81,020 are men and 76,119 women are living in the city (CSA, 2007). Based on the result of housing and population census of from May, 2007 to 2016 the projected population of Hawassa city administration to be 371,826 people out of this 191,352 was male and 180,474 are females. Based on CSA report total number of the population of the city administration 242,489 peoples live in urban area while the reaming129, 337 peoples live in rural areas of the administration. Annual population growth rate 4.02% from this 4.8% growth rate in Urban and 2.8% growth rate in rural areas of the city. Much of the population growth in Hawassa has been the result of internal migration and expansion of Educational and other facilities, also widening of the city boundary has caused some the increased. Hawassa has a young population around 65% of the peoples are under 25 years of age and only about 5.5% of the population is over 50 years of age.(source 2008E.C socio economic profile city administration).

3.5 Wind

This section discusses the wide-area hourly average wind vector (speed and direction) at 10 meters above the ground. The wind experienced at any given location is highly dependent on local topography and other factors, and instantaneous wind speed and direction vary more widely than hourly averages. The average hourly wind speed in Hawassa experiences mild seasonal variation over the course of the year. The winder part of the years for 2.4months, from June 20 to September 1, with average wind speeds of more than 5.0 miles per hour. The windiness day of the year is July 25, with an average hourly wind speed of 6.1 miles per hour. The calmer time of year lasts for 9.6 months, from September 1 to June 20.the calmest day of the year is September 30, with an average hourly wind speed of 3.8 miles per hour. The predominant average hourly wind direction in Hawassa varies throughout the year.

CHAPTER FOUR

4. Data sources and research methods

The analysis including image preprocessing, image classification, land use/land cover indices, the evaluation of LST using thermal bands dataset and the analysis of the relationship between land use/land cover and LST. A flowchart of the research process is described and summarized in (Figure 3.1).

4.1 Data acquisition and materials

In this study, use a series of multi-temporal Landsat imageries such as Landsat 5 Thematic Mapper(TM) and Landsat 8 OLI image were used. These imageries were acquired freely from archive of United States Geological Survey (USGS)[5].

Images were selected at interval of approximately 10 years between 1986 and 2017 for monitoring land use/land cover changes and land surface temperature. All images were acquired during the dry season due to the good availability of cloud free images, but more importantly due to the high relevance of dry season conditions for UHI studies in tropical cities where the highest intensity of UHI commonly occurs during dry or cool seasons (Mcgregor and Nieuwolt, 1998; Roth, 2007).To ensure better comparison of surface temperature and UHI effect all images were acquired in the same month (December) in the winter season. The specific acquisition data of the image was 24, December 1986, 08, December 1998, 09, December 2010 and 28, December 2017 with scenes along the same path. The details of the Landsat data used in the current study are furnished in (Table 4.1).

Image processing, such as image extraction, rectification, atmospheric correction for Landsat data, restoration and classification, and GIS analysis, interpretation and retrieve LST were performed using a set of software to assure higher accuracy: Earth Resources Data Analysis Systems (ERDAS) Imagine 2014, the Environment for Visualizing Images (ENVI 5.1), ArcGIS 10.4.1 (ESRI) software, and IBM SPSS software.

[5](http://earthexplorer.usgs.gov/).

Table 4.1: Satellite data used in the study.

Sensor	Date of Acquisition	Path/Row	Bands	Resolution	Source
Landsat 5 TM	Dec_24_1986	168/055	1_7	30*30	USGS Earth Explorer Website
Landsat 5 TM	Dec_08_1998	168/055	1_7	30*30	USGS Earth Explorer Website
Landsat 5 TM	Dec_09_2010	168/055	1_7	30*30	USGS Earth Explorer Website
Landsat 8 OLI	Dec_28_2017	168/055	1_7and 10 &11	30*30	USGS Earth Explorer Website

4.2 Image pre-processing

Image pre-processing helps to enhance and improve the quality of images. Therefore, sub-section of 20Km by 28Km, covering the entire city of Hawassa and its surrounding rural landscape, were processed to retrieve reflectance from reflective bands of the images and surface temperature from thermal infrared bands. Both Landsat TM and Landsat OLI data are composed of independent single-band images. Therefore, it is necessary to combine these single-band images to a multiband image of TM and OLI using a layer stacking tool.

Atmospheric correction were applied to all image using the Quick Atmospheric Correction (QUAC) algorithm in the ENVI image processing program version 5.1. QUAC is a visible-near infrared through shortwave infrared (VNIR-SWIR) relative atmospheric correction method for multispectral and hyper-spectral imagery. It estimates atmospheric compensation parameters directly from the information contained within the scene (observed pixel spectra) without ancillary information (Bernstein et al., 2005).The raw digital numbers of the thermal bands were converted to Top of Atmosphere (TOA) brightness temperatures using Planck's equation. When data on atmospheric conditions are available, a number of radiative transfer codes (RTCs), such as LOWTRAN and MODTRAN can be used to correct for atmospheric effects and retrieve surface radiance, which can then be converted to Land Surface Temperature (LST) by applying emissivity corrections. The spatial reference system used for all the datasets were WGS 1984 UTM Zone 37N.Therefore, data which were not in this system such as digital aerial photograph, digital topographic maps and other layer of the study area were projected to WGS 1984 UTM Zone 37N.

4.3 Auxiliary Data

Reference data were compiled for each of the four years and use in either classifier training or for accuracy assessment. These data were used to collect sufficient information for image preprocessing, evaluate the ground truth of a certain type of land use/land cover with its imagining characteristics (Omran, 2012), and to determine the major types of land use land cover in the study area. The generated reference data include Hawassa and Shashemena digital topographic maps with a large scale (1:50,000) prepared by National Mapping Agency (EMA), aerial photograph from Hawassa Landholding Registration and Information Office (HLRIO) and Google earth. The spectral signatures of pure pixels of the major urban land use/land cover types are extracted based on the level-I classification scheme of (Anderson, et al., 1976) such as urban (built up), agriculture land, water bodies, vegetation cover and swampy area. The ground truth data and high resolution imagery were in the form of reference data used for assessing accuracy of the classification in addition to points collected during a field survey using Global Positioning System (GPS) receivers.

Figure 4.1: Data processing flow chart showing the general methodology.

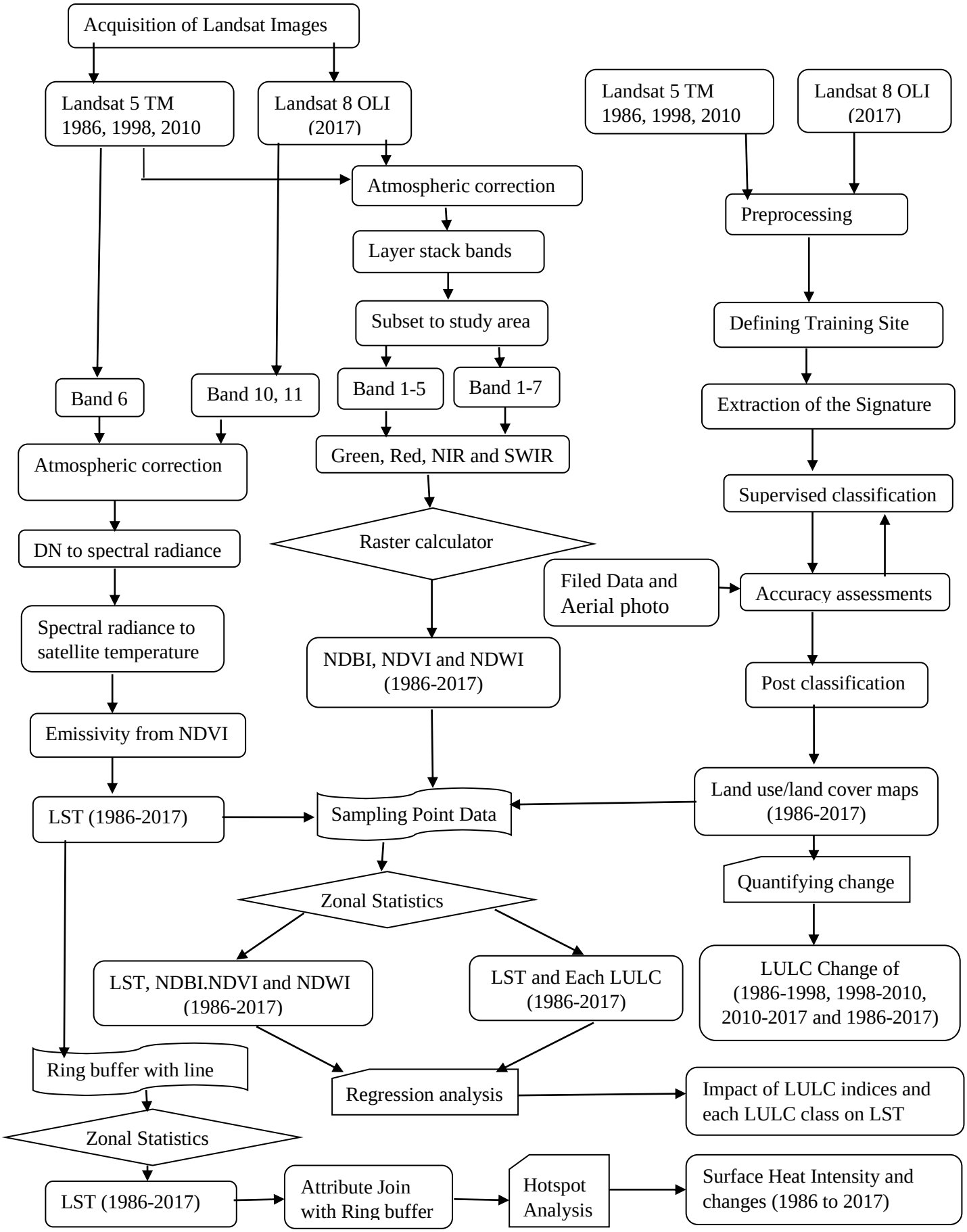

4.4 Land use/land cover classification and accuracy assessment

4.4.1 Classification and accuracy assessment

A classification scheme had to be established before image classification. By computing average spectra of each class, a spectral characteristic of each land use/land cover class in each of the acquired data had been recognized, resulting in a classification schema comprised of five land use/land cover level of classes described in (Table 4.2). For this study, supervise classification was used to create land use/land cover maps, which is considered most common technique of classification approaches (Gillespie, A., 2014).

In this method, the spectral characteristics of the class were defined by identifying training samples. Defined area of interest (AOI) which is called training sample classes and knowledge about the area of interest (AOI) played a vital role in classification process. More than one training samples area was used for a particular land use/land cover class. The training sites were selected from Landsat image with the reference of Google Earth, ground truth data, digital aerial photo and digital topographic maps (Figure 4.2).After the collection of the training samples area, image classification was carried out by using the maximum likelihood classification algorithm. The maximum likelihood classification algorithm assigns a cell to class of the highest probability, where by the probability value was the statistical distance based on the mean values and the covariance and variance of the spectral response patterns of a pixel is the parametric rule used during classification. The basic steps operation followed on supervised classification was:

- Defining the training site:

The first step in undertaking a supervised classification was to define the areas that will be used as training sites for each land use/land cover class. This is usually done by using the on-screen digitized features. The created features are called Area of Interest (AOI).The selection of the training sites was based on those areas clearly identified in all sources of images.

- Extraction of signatures:

After the training site (AOI) was being digitized, the next step was to create statistical characterizations of each information are called Signatures editors in ERDAS Imagine 2014. In this step, the goal was to create a signal (SIG) file for every informational class. The SIG files contain a variety of information about the land use/land cover classes described. After the entire signature has been created then the SIG file saved as dialog box.

- Classification of the image

The supervised classification has been applied after defined training classes. One or more than one training area was used to represent a particular class. During the supervised classification process, the entire signature editor was selected in order to be used on the classification process. Then, the classified was selected from the Editor Menu bar, classify/supervised. Non Parametric rule was used in this classification.

Table 4.2: Classification schema of land use/land cover in the study area.

S.no	LULC types	Description
1	Urban(built-up)	Land covered by buildings and other man-made structures such as residential, commercial services, industrial area,
2	Agriculture	Land covered with temporary crops such as perennial crop, annual crop followed by harvest period, crop fields and pastures
3	Vegetation	Land cover by shrubs, tree and grassland
4	Swampy	Land use by wetland, grass land
5	Water	Land use by lack, river and spring water

Therefore, by the classification processes produce land use/land cover map for the years 1986, 1998, 2010 and 2018. This map showing change for types of land use/land cover classes within the study area and enabled spatio-temporal analysis.

Figure 4.2: Identification of training sites using Landsat Image, aerial photo and Google Earth.

One of the most important final and mandatory steps of image classification process was accuracy assessment. The purpose of accuracy assessment was to quantitatively assess how effectively the pixels were sampled into the correct land use/land cover classes. Moreover, the key emphasis for accuracy assessment pixel selection was on areas that could be clearly identified on both Google earth and aerial photographs.

Reference sample data extraction depends upon two types of sampling units, i.e., pixels (points) and polygons (patches). In this study, the land use/land cover maps were derived by pixel-based image classification so that pixel level sampling units were adopted. Aerial photographs and Google earth were used as sample reference data source for the 1986, 1998 and 2010 land use/land cover classification accuracy assessment. On the other hand, field survey samples were used as reference data for the 2017 land use/land cover classification accuracy assessment. Reference sample size should be kept as small as possible, but still be capable of meeting requirements to assess the accuracy of the classified maps (Gao, 2009). Although various mathematical theories were developed to determine adequate sample sizes for study area (Jensen, 2005; Gao, 2009), no standardized consent has been reached yet regarding the adequate sample size determination. However, a general "rule of thumb" approach is recommended by researchers. According Gao, 2009 proposed that the minimum sample size for each land use/land cover class, necessary for 85% and 90% accuracy interpretation is to be set to 20 and 30, respectively. On the other hand, (Jensen, 2005, Lillesand et al., 2008 and Congalton and Green, 2009) argue that any sample size of less than 50 will be unsatisfactory for error estimations and in most cases a minimum of 50 samples for each map class should be collected for maps of <4,000 km^2 in size and fewer than 12 classes. According to Congalton, 1991 states that 250 reference pixels (±5%) are needed to construct the confusion matrix and to estimate the actual mean of accuracy assessment. Therefore, by considering the size of the study area (560km^2), the identified five land use/land cover classes and to construct the confusion matrix an economical and satisfactory sample size i.e., a minimum of 50 samples per land use/land class was used. The values of the sample points were 482,432,523 and 417 randomly selected reference pixels selected for 1986, 1998, 2010 and 2017 respectively placed on the classified images were generated, representing a specific coordinate of the image. Among other sampling techniques, a stratified random sampling scheme was used to generate reference sample datasets. The main advantage of this type of sampling scheme for this study is that no matter how small a land use/land cover class is in size or limited in its spatial extent, smaller areas can be adequately represented (Gao, 2009).

Therefore, the accuracy of classification was verified by the filed checking and comparing with the existing land use/land cover. The most common method generally used for the accuracy assessment was the error matrix (Confusion Matrix). Confusion matrices were computed to evaluate the relationship between the reference data used and the resulting classified land use/land cover maps. The arrangement of the error matrix was numbers representing number of samples assigned to a specific category relative to the ground truth, in

rows and columns. The rows in the matrix represents classification derived land use/land cover maps while columns represent reference data collected from the field data, Google earth and aerial photograph. This matrix enables computations of several statistical measures such as overall accuracy like producer's and user's accuracy and kappa coefficient (Congaltion and Green, 2009).

The overall accuracy is defined as the ratio of the number of correctly classified pixels (i.e. the sum of the diagonal elements) to the total number of pixels checked, expressed in percentage.

$$\text{The overall classification accuracy} = \frac{\text{Number of Correct Points}}{\text{Total Number of Points}} \qquad (4.1)$$

However, the overall accuracy is an average, so it does not expose how error was distributed between the classes. Therefore, in this research consider other metrics derived from the error matrix to further describe accuracy assessments including; Commission and omission error, sensitivity and specificity and kappa statistics. This statistical related classification accuracy was computed based on the following formula.

$$\text{Sensitivity} = \frac{a}{a+b}\,(\text{Equivalent to Producer}'s) \qquad (4.2)$$

$$\text{Specificity} = \frac{d}{b+c} \qquad (4.3)$$

Where: a=Number of times a classification agreed with the observed value.

b=Number of times a point was classified as X when it was observed to not be X.

c=Number of times a point was not classified as X when it was not observes to be X.

Error Commission were the percentage of pixels placed in a given category when they actually belong to the other category.

$$\text{Commision Error} = 1 - \text{Specificity} \qquad (4.4)$$

Errors of omission were the percentage of pixels that should have been put into a given category but were not.

$$\text{Ommision error} = 1 - \text{Sensitivity} \qquad (4.5)$$

The Kappa statistics reflects the difference between actual agreements expected by chance. It incorporates the off diagonal of the error matrix (Foody, 2002; Lillesand et al., 2007; Tempfli, 2009) or KAPPA analysis is a discrete multivariate technique used in accuracy assessments (Jensen, J.R., 1996). Kappa analysis yields a Khat statistics (an estimate of KAPPA) that is a measure of agreement or accuracy (Congalton, R.G., 1991).the Khat statistics is computed as;

$$K = \frac{N\sum_{i=}^{r} x_{ii} - \sum_{i=1}^{r}(x_i + X_{x+1})}{N^2 - \sum_{i=1}^{r}(x_{ii} X_{x+1})} \quad (4.6)$$

Where: r=Number of rows and columns in the error matrix,

N=total number of observation (pixels).

X_{ii} = observation in row i and column i

X_{i+} = marginal total of row i, and X_{+i} = marginal total of column i

A Kappa coefficient equal to 1 means perfect agreement where as a value close to zero means that the agreement is no better than would be expected by chance.

According to Landis, J.R. and Koch, G.G., 1977 categorization of Kappa statistic divide into six range.

Table 4.3: Category of Kappa Statistics.

S.no	Kappa statistics	Strength of agreement
1	<0.00	Poor
2	0.00-0.20	Slight
3	0.21-0.40	Fair
4	0.41-0.60	Moderate
5	0.61-0.80	Substantial
6	0.81-1.00	Almost Perfect

4.4.2 Estimation of percent LULC and change analysis

A classification comparison change detection method was used to evaluate dynamics of land use/land cover in the area of interest (Ridd, and Liu, J., 1998).In order to analyses the nature, rate and location of urban land use/land cover change, an image of urban and rural land use land cover was extracted from each original land cover images. Therefore, four change detection statistics were obtained over time from the independent classified images for this research by conducting cross-tabulation analysis on a pixel-by-pixel basis, i.e. thematic overlay of the classified images (Al-Bakri, et al., 2013).Changes were detected for time intervals of roughly ten years: 1986–1998, 1998–2010, 2010–2017. In addition, the time range of 1986-2017 was included to examine the overall change over the past 30 years. To evaluate the matrix table of “from-to” change information that revealed the main gains and losses in each category to obtain an urban landscape expansion.

4.5 Land use land cover indices

4.5.1 Normalized Difference Vegetation Index (NDVI)

Normalized Difference Vegetation Index (NDVI) is the most commonly used index to express information about the density of vegetation, predicate crop production, monitor drought, map desert encroachment (Xiong, et al., 2012) and measure surface radiant temperature (Omran, 2012). NDVI is the difference of near infrared and visible red reflectance values normalized over reflectance and calculated from reflectance measurements in the near infrared (NIR) and red portion of the spectrum (Burgan and Hartford, 1993). To calculate the Normalized Difference Vegetation Index (NDVI), subtracting the red band from near infrared band and then dividing to near infrared band plus red band (Eq., 4.7). The value is ranging from -1 to 1, the negative values are indicative of water, snow, clouds, non-reflective surface and other non-vegetated, while the positive value expresses reflective surfaces such as vegetated area (Burgan and Hartford 1993). NDVI use Landsat 5 TM the reflectance in the Near-infrared band (0.76-0.9μm) and red band (0.63-0.69μm) and for Landsat 8 OLI Near-infrared band (0.85-0.88μm) and red band (0.64-0.67μm).

Mathematically, NDVI were calculated using the following formula:

$$\mathrm{NDVI} = \frac{\mathrm{NIR} - \mathrm{R}}{\mathrm{NIR} + \mathrm{R}} \qquad (4.7)$$

Where: NDVI-Normalized Difference Vegetation Index

NIR-Near-Infrared Band

R- Red Band

4.5.2 Normalized Difference Built-up Index (NDBI)

NDBI was first developed by (Zha, Y., Gao, J. and Ni, S., 2003) to investigate the extent and density of imperviousness surface and built-up areas and map these areas, as it can highlight the urban distribution with a typically higher reflectance in the short-wave infrared region band than that of the near-infrared one (Alhawiti, R.H. and Mitsova, D., 2016).The NDBI separates built-up from other ground cover. Its ratio was calculated through the difference of Short-wave Infrared Band (SWIR) and Near Infra-red (NIR) which was normalized by summing up these two bands (eq., 4.8). NDBI use NIR and SWIR are the reflectance in the Near-Infrared band (0.76 -0.9 μm) and Short-wave Infrared band (1.55 - 1.75 μm), respectively, for Landsat 5 TM. However, for Landsat 8 OLI these differed slightly: Near-Infrared band (0.85 - 0.88 μm) and Short-wave Infrared band (1.57 - 1.65 μm).

$$\mathrm{NDBI} = \frac{\mathrm{SWIR} - \mathrm{NIR}}{\mathrm{SWIR} + \mathrm{NIR}} \quad (4.8)$$

Where: NDBI-Normalized Difference Built-up Index

SWIR-Short Wave Infrared Rad,

NIR-Near-Infrared Band

4.5.3 Normalized Difference Water Index (NDWI)

NDWI is an index to extract water bodies from satellite imagery. The NDWI indices value from -1 to 1. NDWI has been developed to delineate open water and enhanced their presence in remote sensed imagery based on reflected near infrared radiation and visible green light. NDWI may allow turbidity of water bodies to be estimated from remote sensed data (McFeeter, 1996). NDWI is sensitive to change in liquid water content of vegetation canopies.

Water has a high reflectance in the Short Wave Infrared Red (SWIR) and Green band of a sensor system. The NDWI separates water from other water cover. Its ratio was calculated through the difference of Green (G) and Short Wave Infrared Red (SWIR) which was normalized by summing up these two bands using (Eq., 4.9).NDWI use Green and SWIR are the reflectance in the Green band (0.52 - 0.60 µm) and Short-wave Infrared band (1.55 - 1.75 µm), respectively, for Landsat 5 TM. However, for Landsat 8 OLI these differed slightly: Near-Infrared band (0.85 - 0.88 µm) and Short-wave Infrared band (1.57 - 1.65 µm).

$$\mathrm{NDWI} = \frac{\mathrm{G} - \mathrm{SWIR}}{\mathrm{G} + \mathrm{SWIR}} \quad (4.9)$$

Where: NDWI-Normalized Difference Water Index

SWIR-Short Wave Infrared Rad,

G- Green Band

4.6 Land surface temperature retrieval

Table 4.4 present all the parameters introduced in this section. Land surface temperature was estimated from the thermal infrared bands of different types Landsat images such as band 6 for Landsat 5 TM and band 10 and 11 for Landsat 8 OIL. The basic steps for the retrieval of land surface temperature given below are based on the guideline provided in Landsat data Handbook published by USGS[6].

[6] (https://landsat.usgs.gov)

Table 4.4: The parameters in land surface temperature.

S.No	Parameters	Definition
1	$\frac{L_{\lambda}}{L_{TOA}}$	The spectral at-sensor radiance(top of the atmosphere)
2	$G_{re\_secaled}$	The rescaled gain (the data product "gain" contained in the Level 1 product header or ancillary data record)
3	$B_{re\_secaled}$	The rescaled bias (the data product "offset" contained in the Level 1 product header or ancillary data record)
4	Q_{cal}	The quantized calibrated pixel value
5	$L_{Min,\lambda}$	The spectral radiance scaled to QCALMIN
6	$L_{Max,\lambda}$	The spectral radiance scaled to QCALMAX
7	$Q_{cal,Min}$	The minimum quantized calibrated pixel value (corresponding to $L_{Min,\lambda}$)
8	$Q_{cal,Max}$	The maximum quantized calibrated pixel value (corresponding to $L_{Max\lambda}$)
9	M_L	the radiance multiplicative scaling factor for the band (Radiance_multi_band from the metadata
10	Δ_L	The radiance additive scaling factor for the band (Radiance_multi_band from the metadata)
11	τ	The atmospheric transmission
12	ε	The emissivity of the surface
13	L_T	The radiance of a blackbody target of kinetic temperature T
14	L_u	The upwelling or atmospheric path radiance
15	L_d	The down welling or atmospheric path radiance
16	T	The apparent surface temperature in Kelvin
17	K_1,K_2	The calibration constants

Atmospheric correction was first required to eliminate the atmospheric effect from thermal bands, as the satellite imagery measures the radiance of surface features modified by the atmosphere (Li, et al., 2014). Therefore, the Top of Atmospheric (TOA) radiance correction model was applied on Landsat 5 TM imageries for both 1986, 1998 and 2010. TOA radiance is a simple model based on the scene calibration data available from the imagery header file.

1. Conversation pixel value to TOA radiance

The pixel values were converted from the Digital Number (DN) units to radiation values for Landsat 5 and Landsat 8 OLI.

For Landsat 5 TM: Based on (Chander, G. and Markham, B., 2003), brightness temperature from Landsat 5 can be obtained first by the conversion of the digital number of band 6 to Top of Atmospheric (TOA) radiance using the following equation.

$$L_{\lambda} = G_{rescale} * Q_{cal} + B_{rescale} \quad (4.10)$$

This can be expressed as:

$$L_{\lambda} = \frac{L_{max\lambda} - L_{Min\lambda}}{Q_{calmax} - Q_{calmin}} * (Q_{cal} - Q_{calmin}) + L_{min\lambda} \quad (4.11)$$

Where: L_{λ} - TOA radiance

MAX L_{λ} is highest radiance corresponding to MAX Cal Q (DN = 255),

MIN L_{λ} is lowest radiance corresponding to MIN Cal Q (DN= 0), and

Cal Q is the quantized calibrated pixel value of band 6 in DNs.

For Landsat 8 OLI: In the case of Landsat 8, TOA spectral radiance was computed using the radiance rescaling factors corresponding to each band provided in the metadata file using the following equation (Zanter, K, 2016).

$$L\,\lambda = M_L Q_{cal} + A_L \quad (4.12)$$

Where: L λ- TOA spectral radiance, (watts/ (m^2*s rad*μm))

M_L-Band-Specific multiplicative rescaling factors from the metadata (Radiance_multi_Band x, where x is the band number)

A_L- Band-Specific Additive rescaling factors from the metadata (Radiance_multi_band x, where x is the band number)

Q_{cal}- Quantized and calibrated standard product pixel values (DN)

2. Estimation of a sensor brightness temperature or conversion of spectral radiance to at sensor brightness temperature.

Table 4.5: Landsat thermal band calibration constant.

Satellite	Band number	K_1 (W/m^2*sr*μm)	K_2 (Kelvin)	$L_{\lambda\,MAX}$ (W/m2*sr*μm)	$L_{\lambda\,MIN}$ (W/m2*sr*μm)
Landsat 5	6	607.76	1260.56	1.2378	15.303
Landsat 8	10	774.8853	1321.0789		
Landsat 8	11	480.8883	1201.1442		

TIRS band data can be converted from radiance to brightness temperature using the thermal constants providing in the metadata file. The spectral radiance of thermal infrared bands was converted into active radiance at sensor brightness temperature (the temperature values of black body) using Planck's function equation as follows:

$$T_i = \frac{C_2}{(\lambda_i * \ln(1 + \frac{C_1}{L_i \lambda_i^5}))} \quad (4.13)$$

Where: T_i-represents sensor brightness temperature in kelvin

C_1 and C_2 are constants; C_1=1.19104356*10^{-16}W.m^2, C_2=1.4387685*$10^4 \mu m$K.

λ_i Emitted radiance wavelength for peak response and average limiting wavelengths.

This equation was simplified to the following form and used to convert Landsat data (Al Kuwari et al., 2016, Chander and Markham, 2003 and Van and Bao, 2010).

$$T_i = \frac{K_2}{\ln(\frac{K_1}{L_\lambda} + 1)} \quad (4.14)$$

Where: T_i-At-satellite brightness temperature (K)

L_λ-TOA spectral radiance, (watts/ (m^2*s rad*μm))

K_1 - a calibration constant 1, and

K_2 - a calibration constant 2 in Kelvin (Table 3).

3. Determination of land surface emissivity

Land surface emissivity affects the satellite measurements by three categories:

i) Emissivity causes a reduction of surface-emitted radiance;

ii) Non-black surfaces reflect radiance; and

iii) Anisotropy of reflectivity and emissivity might reduce or increase total surface radiance.

Emissivity as a function of wavelength is controlled by several environmental factors such as surface water content, chemical composition, structure, and roughness. For vegetated areas, emissivity varies significantly with plant species, areal densities, and growth rates. In fact, land surface emissivity is closely related to NDVI (Weng and Larson, 2005; Van and Bao, 2010). Therefore, the emissivity can be estimated from NDVI used.

$$P_V = (NDVI - NDVI_{min}/NDVI_{max} - NDVI_{min})^2 \quad (4.15)$$

P_V=Proportion of vegetation

$$\varepsilon = 0.004P_V + 0.986 \quad (4.16)$$

4. Land surface temperature estimation

The emissivity-corrected land surface temperature was obtained using the following equation (Xiong et al., 2012; Yue et al., 2012):

$$T_S = \frac{T_i}{1 + \left(\lambda * \frac{T_i}{\rho}\right) * \ln \varepsilon} \quad (4.17)$$

Where: T_S -represents land surface temperature,

T_i -indicates sensor brightness temperature in Kelvin,

λ -the wavelength of the emitted radiance (for peak response and average limiting wavelengths),

ε-land surface spectral emissivity.

$\rho = \frac{h_c}{\sigma}$= 1.438*10^{-2}mk,

Where: h_c is Plank's constant (6.626*10^{-34}Js),

C indicates light velocity (2.998*10^{8}m/s), and

σ - The Boltzmann constant (5.67*10^{-8}Wm^{-2}k^{-4}=1.38*10^{-23}J/k).

5. Convert land surface temperature value from kelvin unit to degree Celsius

$$\mathrm{LST}(0_{\mathrm{celsius}}) = \mathrm{LST}(\mathrm{Kelvin}) - 273.15 \quad (4.18)$$

4.7 Relationship between LST and LULC

A single liner regression analysis was the statistical process useful for estimating the relationship among single explanatory variables (Independent) and a predictor (Dependent variable) (Higgins, 2005). single liner regression analysis were initially applied to determine the correlation between land surface temperature and land use/land cover types and land use/land cover indices. Normalized Difference Vegetation Index (NDVI), Normalized Difference Built-up Index (NDBI) and Normalized Difference Water Index (NDBI and LST values were extracted from each pixel in the study area for each sampling point by the use of zonal statistics tools in ArcGIS software. These points were used as the input for the linear regression model. This model gives a general idea about the correlation/relationship between LST and land use/land cover types and indices.

It is the generalization of linear regression to multiples which can be expressed as:

$$Y_i = \beta_0 + \beta_1 * X_{i1} + \beta_2 * X_{i2} + \cdots + \beta_r * X_{ir} + \varepsilon_i \quad (4.19)$$

Where: we consider n number of observations of one predicator and r explanatory variables.

Y_i=ith observation of the predictor

X_{ij}=ith observation of the jth explanatory variable (j=1, 2, 3,……, r)

β_j=Parameters to be estimated

ε_i=ith independent identically distributed normal error

For the regression analysis between the LST and land use land cover types and land use land cover indices use simple random sampling methods. 250 sample pointes use for each land use land cover types and 500 sample pointes use for land use land cover indices.

4.8 Surface Heat Intensity (SHIn) and change analysis

Two methods were used to estimate daytime surface thermal intensity and spatial/temporal variation using thermal bands of Landsat satellites: thermal gradient analysis and hotspot analysis. To analyze the thermal intensity of the study area by using multiple ring buffer tools in GIS environment. The study area was sub divided with regard to distance and direction like a spider-web pattern. The study area divides in 32 radial directions and with 30 circular zones arranged by the proximity to the central point of the city and then clip by the boundary of study area. The circular zones are designed in such a way that all radial sections are zonal areas. Surface Heat Intensity (SHIn) of each land use land cover types are calculated for each sub-section of the spider web pattern. The benefit of sub dividing the urban and surrounding rural areas into distance and direction categories into two reasons: first, it enables detailed analysis of spatial pattern of the surface heat intensity of the study area. And secondly, it calculates the temporal variation the Surface Heat Intensity (SHIn) of four years.

In this research use the hot spot analysis to quantify Surface Heat Intensity (SHIn) and to examine its spatial pattern over 30 years. Hotspot analysis tool in the ArcGIS software, developed by Environmental System Research Institute (ESRI) was applied to explore thermal accumulation in different parts of the city, and to examine thermal variation among urban and rural landscapes. The spatial pattern and statistical significance of thermal clustering was evaluated through the Getis-Ord Gi*Zscore (Eq., 24). The hot spot analysis tools calculate the Getis-Ord Gi* statistic for each feature in a data base. The resultant Z-score and P- Value tell you where feature with either high or low values cluster spatially. It was to identify statistically significant of the features with higher positive z-score shows

more intense or clustering of high values (hot spot) and smaller negative z-score represents more intense clusters of low values (cold value) and the feature with high value may not be statistically significant over an entire area by looking at each feature from our land surface temperature value within the context of its neighboring features (Ord and Getis, 1995).

The Gi*Zscore the output feature class also contained p-value and confidence level bin (GI_Bin). A high z-score and small p-value for feature would indicate spatial clustering of high values. On the other hand, a low negative z-score and a small p-value would indicate spatial clustering of low values (ESRI, 2016).From the statistics results, we defined magnitude of intra_Urban thermal difference as surface Heat Intensity (SHIn) and we quantified SHIn as mean temperatures difference between hotspot and cold spot area. The surface heat intensity the pattern was divided into seven categories: very hot spot, hot spot, warm spot, not statistically significance, cool spot, cold spot and very cold spot.

Gi*Zscore values of 2.58 and -2.58, which correspond to the 99% confidence level, were chosen to identify area characterized by significant aggregation of high temperature that is hotspot and low temperature that is cold spot, respectively. This approach to quantifying thermal intensity not only account for differences in temperature but also for the statistical significant of aggregation at the chosen measure of connectivity.

The Gi*Zscore is given by:

$$G_i * = \frac{\sum_{j=1}^{n} W_{i.j}, X_j - X \sum_{j=1}^{n} W_{i,j}}{S\sqrt{\frac{[n\sum_{j=1}^{n} W_{i,j}{}^2 - (\sum_{j=1}^{n} W_{i,j})^2]}{n-1}}} \quad (4.20)$$

$$X = \frac{\sum_{j=1}^{n} X_j}{n} \quad (4.21)$$

$$S = \sqrt{\frac{\sum_{j=1}^{n} x_j{}^2}{n} - (X)^2} \quad (4.22)$$

Where: $W_{i,j}$ is spatial weight based on Queen's adjacency connectivity matrix's between reference point i and n points within defined distance from point i, X_j is temperature value at point j and X is mean of temperature values.

$$SHIn = Tmean_{Gi*Zscore>2.58} - Tmean_{Gi*Zscore<-2.58} \quad (4.23)$$

Where: SHIn is surface heat intensity

$Tmean_{Gi*Zscore>2.58}$ is the mean surface temperature of area with greater than 2.58,and similarity $Tmean_{Gi*Zscore<-2.58}$ is the mean surface temperature of area with less than -2.58.

CHAPTER FIVE

5. Results and Discussion

5.1 Spatial distribution pattern and accuracy assessment of LULC

The land use/land cover classification of the area for 1986 from Landsat TM satellite image. The area of each class was calculated taking into account the pixel count and total area (study area). Thus allocations of each classified area and percentage are tabulated in (Table 5.1). The percentage of areas as classified are; urban (built-up) areas 5.95 %, agriculture land 33.36 % ,vegetation cover 34.89 %, swampy 9.59 % and water bodies 16.21%. The spatial distribution patterns reveal that the area was dominated by agriculture land and vegetation cover, vegetation cover located in the north east and south east region and urban (built-up) area in the middle (Figure 5.1).

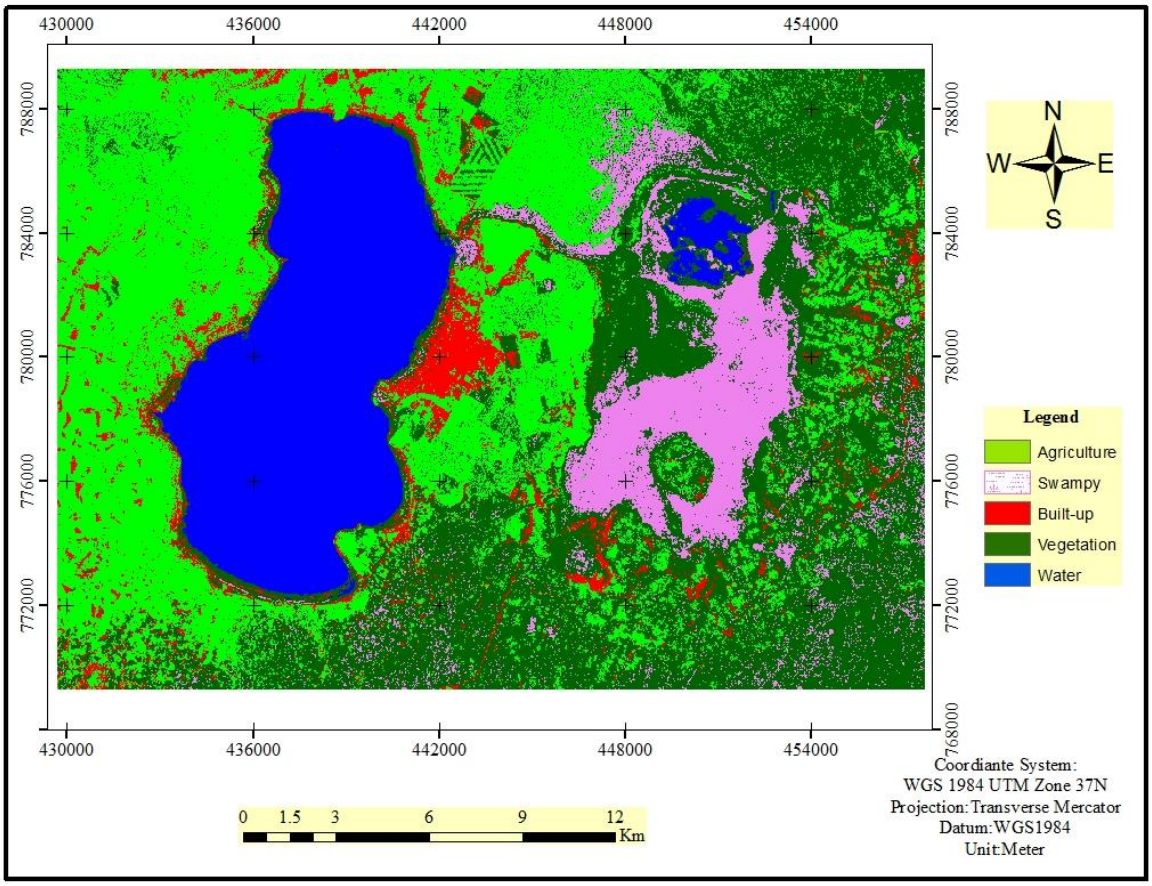

Figure 5.1: Land use/land cover map produced by classification processes showing types of classes within the study area in 1986.

The land use/land cover classification of the area for 1998 from Landsat TM satellite image. The allocations of each classified area, (percentage) are tabulated in (Table 5.1). The percentage of areas as classified are; urban (built-up) areas 6.16 %, agriculture land 38.19 %

,vegetation cover 27.32 %, swampy 12.65 % and water bodies 15.68 %. The spatial distribution patterns reveal that the area was dominated by agriculture land and vegetation cover, vegetation in the northeast and southwest region and urban (built-up) area in the middle (Figure 5.2).

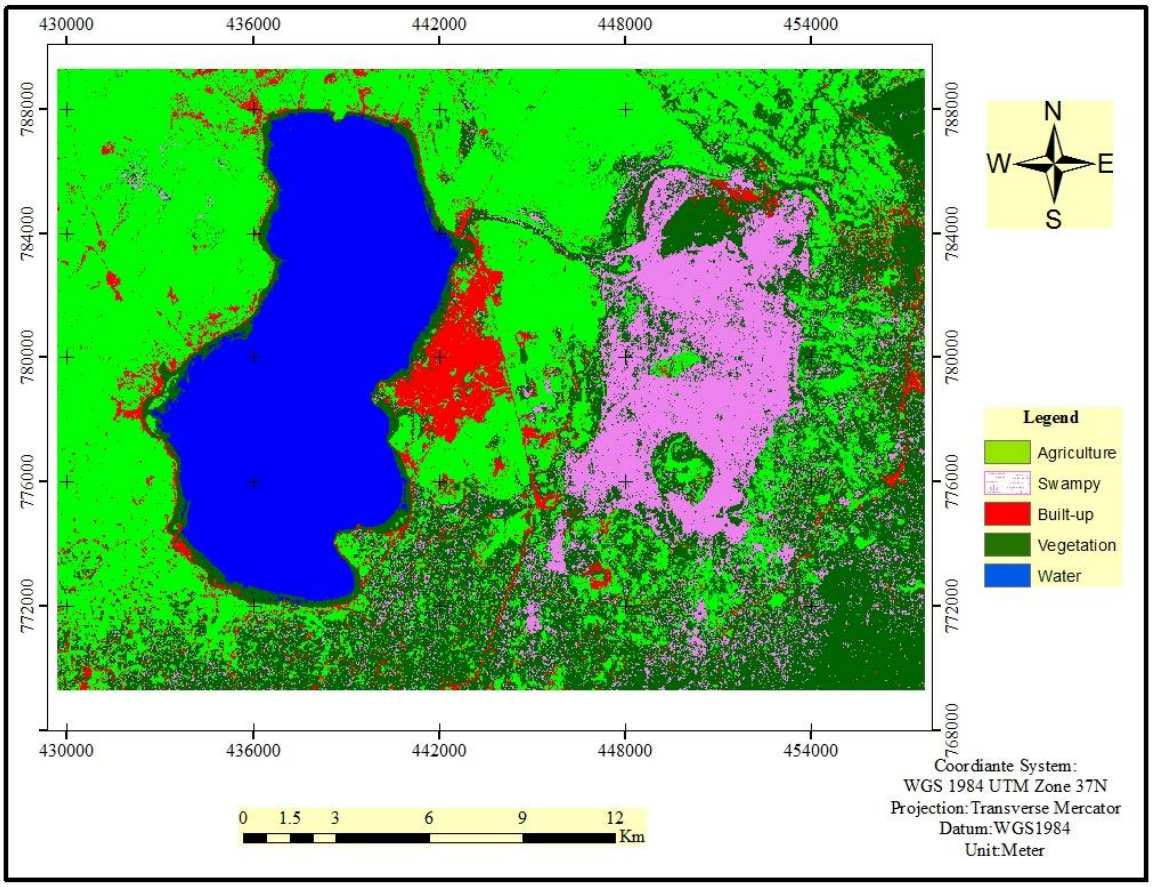

Figure 5.2: Land use/land cover map produced by classification processes showing types of classes within the study area in 1998.

The land use/land cover classification of the area for 2010 from Landsat TM satellite image. The allocations of each classified area, (percentage) are tabulated in (Table 5.1). The percentage of areas as classified are; urban (built-up) areas 9.44 %, agriculture land 35.25 % ,vegetation 28.79 %, swampy 11.15 % and water bodies 15.38 %. The spatial distribution patterns reveal that the area was dominated by agriculture land and vegetation cover, vegetation in the northeast and southwest region and urban (built-up) area in the middle (Figure 5.3).

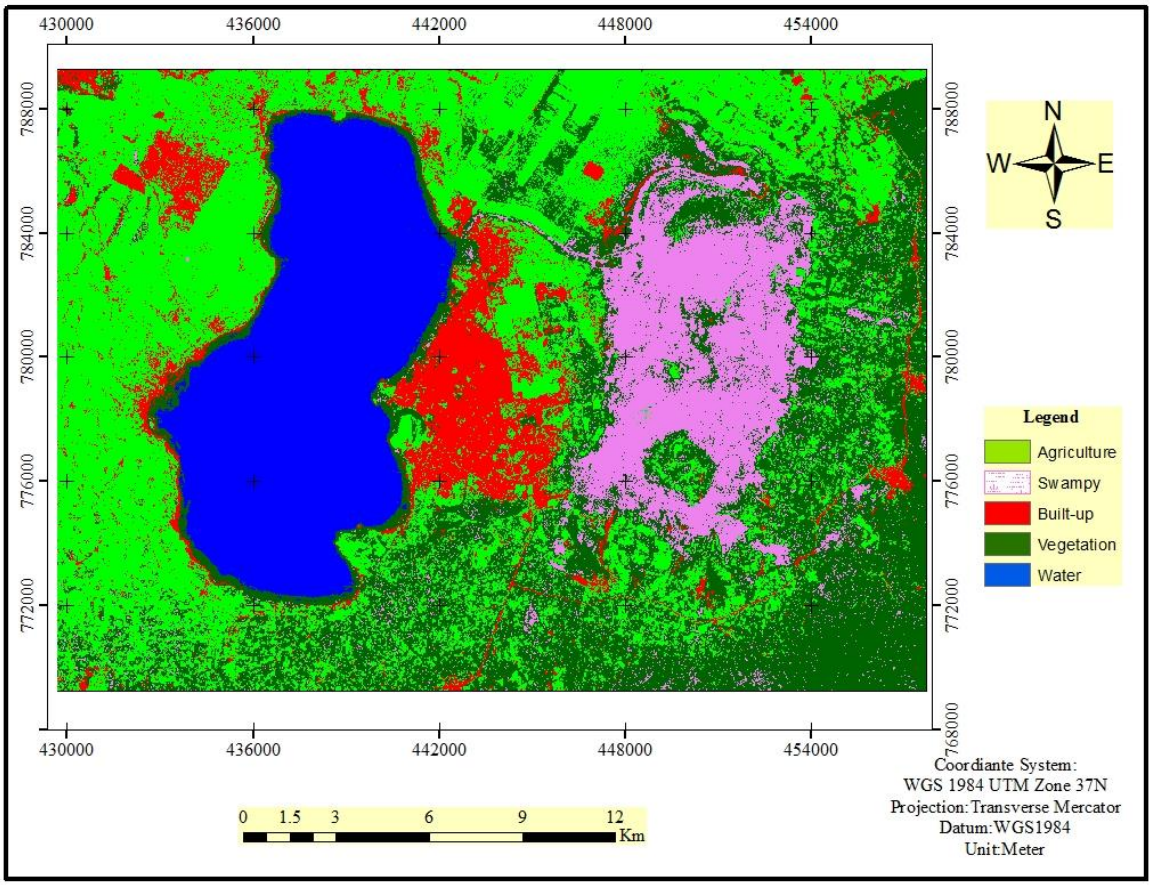

Figure 5.3: Land use/land cover map produced by classification processes showing types of classes within the study area in 2010.

The land use/land cover classification of the area for 2017 from Landsat TM satellite image. The allocations of each classified area, (percentage) are tabulated in (Table 5.1). The percentage of areas as classified are; urban (built-up) areas 13.2 %, agriculture land 31.53 % ,vegetation 31.87 %, swampy 8.51 % and water bodies 14.89 %. The spatial distribution patterns reveal that the area was dominated by agriculture land and vegetation cover, vegetation in the northeast and southwest region and urban (built-up) area in the middle (Figure 5.4).

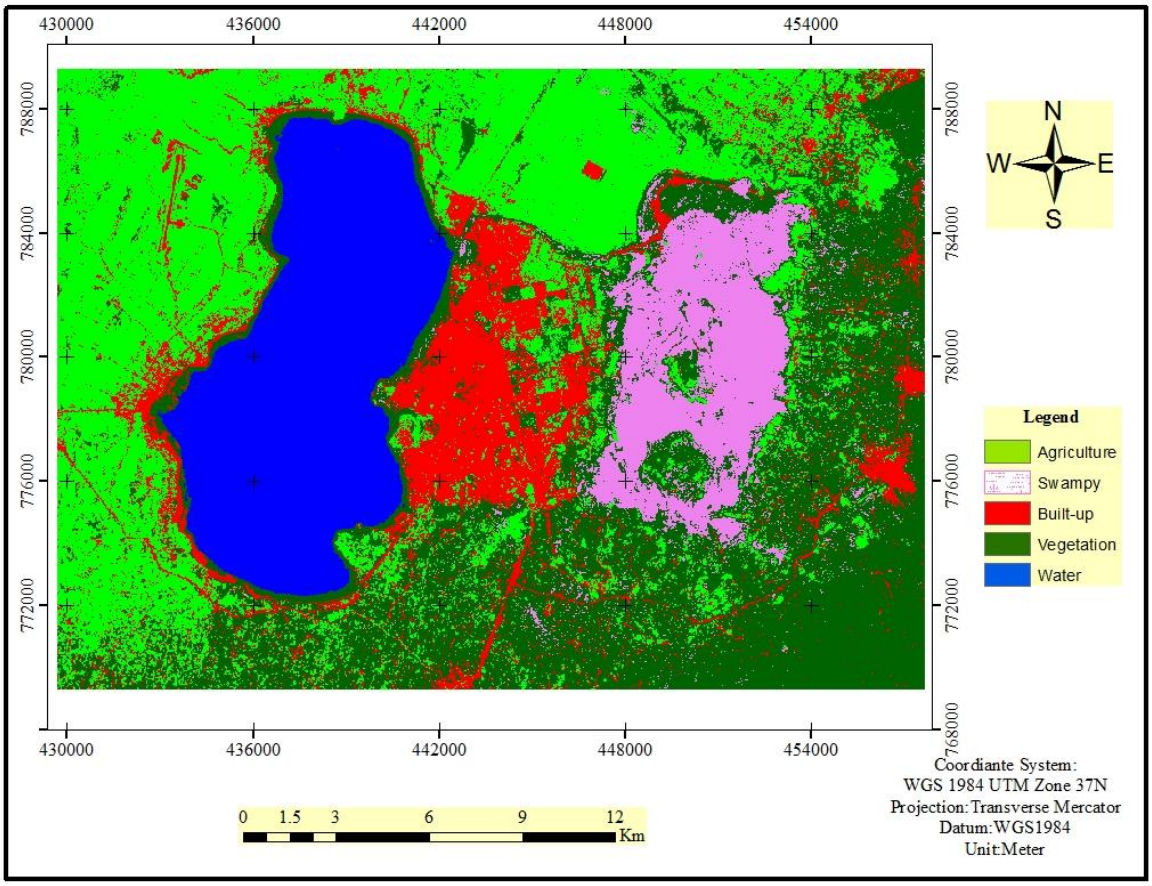

Figure 5.4: Land use/land cover map produced by classification processes showing types of classes within the study area in 2017.

Table 5.1: Area statistics of land use land cover classes for 1986 to 2017.

		1986		1998		2010		2017	
S.no	LULC type	Area(Km^2)	%	Area(Km^2)	%	Area(Km^2)	%	Area(Km^2)	%
1	Urban(built-up)	33.31	5.95	34.51	6.16	52.88	9.44	73.84	13.2
2	Agriculture	186.87	33.36	213.08	38.19	197.44	35.25	176.56	31.53
3	Vegetation	195.40	34.89	153.01	27.32	161.09	28.79	178.18	31.87
4	Swampy	53.71	9.59	70.87	12.65	62.45	11.15	47.6	8.51
5	Water	90.79	16.21	87.8	15.68	86.2	15.38	83.38	14.89
	Total	560	100	560	100	560	100	560	100

Generally, Table 5.1 presented the area estimates for the land use land cover class of the study area derived from the classification results. Among all land use land cover types, agriculture land constituted predominate types in all four years and vegetation land cover types was the second largest land use land cover class in all years. On the other hand, water bodies and swampy land cover types also constitute a significant portion of the land use land cover units of the study area. The smallest land use land cover class were urban (built-up) area but dramatic increase in area from 4.8 percent the total area in 1986 into 13.20 percent of the total area in 2017.

Classification accuracy assessment: for this analysis, 482 and 548 reference samples, derived from aerial photo interpretation were used to validate 1986 and 2010 land use/land cover classifications, respectively (Tables 5.2 and 5.4), whereas the 1998 classification was tested using 565 sample points derived from Google earth and 2017 using field survey ground truth data (Table 5.3 and 5.5).

Various accuracy assessment evaluating parameters were computed in the classified image such as user's accuracy, procedural's accuracy and overall accuracy. The user's accuracy reflects the reliability of the classification to the user. User's accuracy was the more relevant measure of the classification's actual utility in the field. The measure of producer's accuracy (Sensitivity) reflects the accuracy of prediction of the particular category. The commission error reflects the points which are included in the category while they really do not belong to the category. The omission error reflects the number of points which are not included in the category while they really belong to the category.

Error matrices for year 1986 classification are presented in Tables 5.2. The results from error matrices showed overall accuracy obtained from the stratified random sampling process for the classified image of 1986 were 92.95 % (Eq., 4.1). The user's and producer's accuracies are ranging from 86.02 % to 100 % in 1986 and from 81.63% to 100%. Urban (built-up), swampy and water bodies had the highest producer's and user's accuracy greater than 90%.The commission error in 1986 was highest (0.14) in the case of vegetation cover which mean that more number of points (13) which do not fall under this category are classified as vegetation land use/land cover. The omission error in the case of vegetation cover was highest (3.18) with 18 points which actually belong to this category not being categorized in this class (Table 5.2).

Table 5.2: Error matrix of the 1986 land use/land cover classification of the study area.

Classified data	Reference data							
	Built-up	Agriculture	Vegetation	Swampy	Water	total	UAcc. (%)	Cerr.
Built-up	92	3	3	0	0	98	93.88	0.06
Agriculture	0	97	15	0	0	112	86.61	0.13
Vegetation	0	2	80	10	1	93	86.02	0.14
Swampy	0	0	0	90	0	90	100.00	0
Water	0	0	0	0	89	89	100.00	0
Total	92	102	98	100	90	482	OAcc=92.95%	
PAcc. (%)	100	95.1	81.63	90	98.89		(K^) =0.91	
Oerror	0	0.03	3.18	0.1	0.01			

Note: UAcc. =User's Accuracies, PAcc. Producer's Accuracies, OAcc. =Overall accuracy, K^ = Kappa Statistics, Cerr= Commission error and Oerror= Omission error

Based on error matrix for 1998, the user's and producer's accuracies are ranging from 84.76 % to 100 % in 1986 and from 90.48 % to 97.80 % respectively (Eq., 4.1). Urban (built-up), swampy, water bodies and agriculture land cover had the highest user's accuracy greater than 95 %. All land uses/land cover class had the highest producer's accuracy (Table 5.3). The commission error in 1998 was highest (0.15) in the case of vegetation cover which mean that 16 points do not fall under this category are classified as vegetation land use(Eq., 4.4). The omission error in the case of water bodies was highest (0.08) with 7 points which actually belong to this category not being categorized in this class (Eq., 4.5).

Table 5.3: Error matrix of the 1998 land use/land cover classification of the study area.

Classified data	Reference data							
	Built-up	Agriculture	Vegetation	Swampy	Water	Total	UAcc. (%)	Cerr
Built-up	66	2	0	0	0	68	97.06	0.09
Agriculture	0	114	1	2	1	118	96.61	0.03
Vegetation	2	2	89	5	7	105	84.76	0.15
Swampy	1	0	1	87	0	89	97.75	0.02
Water	0	0	0	0	76	76	100.00	0
Total	69	118	91	94	84	456	OAcc=94.74%	
PAcc. (%)	95.65	96.61	97.80	92.55	90.48		(K^) =0.93	
Oerror	0.04	0.03	0.02	0.08	0.10			

Note: UAcc. =User's Accuracies, PAcc. Producer's Accuracies, OAcc. =Overall accuracy, K^ = Kappa Statistics, Cerr= Commission error and Oerror= Omission error

The overall accuracy for the 2010 was 95.44% with Kappa statistics agreement of 0.94, which is better than 1986 land use/land cover classification (Eq., 4.1 and Eq., 4.6). The user's and producer's accuracies are ranging from 87.39 % to 100 % and from 91.58 % to 97.44% respectively. Except vegetation land class (87.39%), all land use/land cover categories have high user's accuracies of more than 90%. All land uses/land cover class had the highest producer's accuracy greater than 90% (Table 5.4). The commission error in 1998 was highest (0.13) in the case of vegetation land cover type which mean that 14 points do not fall under this category are classified as vegetation land cover(Eq., 4.4). The omission error in the case of water bodies was highest (0.05) with 5 points which actually belong to this category not being categorized in this class (Eq., 4.5).

Table 5.4: Error matrix of the 2010 land use/land cover classification of the study area.

Classified data	Reference data							
	Built-up	Agriculture	Vegetation	Swampy	Water	Total	UAcc. (%)	Cerr
Built-up	129	1	2	0	0	132	97.73	0.03
Agriculture	4	96	2	0	0	102	94.12	0.06
Vegetation	0	3	97	3	8	111	87.39	0.13
Swampy	0	1	1	114	0	116	98.28	0.02
Water	0	0	0	0	87	87	100.00	0
Total	133	101	102	117	95	548	OAcc=95.44%	
PAcc. (%)	96.99	95.05	95.10	97.44	91.58		(K^) =0.94	
Oerror	0.03	0.04	0.05	0.03	0.084			

Note: UAcc. =User's Accuracies, PAcc. Producer's Accuracies, OAcc. =Overall accuracy, K^ = Kappa Statistics, Cerr= Commission error and Oerror= Omission error

The computed user's and producer's accuracy values of year 2017 classification, range from 89.74 % to 100 % and from 91.67 % to 100% respectively. Except vegetation land use class (87.39%), all land use/land cover categories have high user's accuracies of more than 90%. The user's accuracy of vegetation land use types is the lowest (87.39%) (Table 5.5). The commission error in 2017 was highest (0.1) in the case of vegetation land cover types which mean that 8 points do not fall under this category are classified as vegetation land cover class(Eq., 4.4). The omission error in the case of agriculture land was highest (0.08) with 7 points which actually belong to this category not being categorized in this class (Eq., 4.5).

Table 5.5: Error matrix of the 2017 land use/land cover classification of the study area.

Classified data	Reference data							
	Built-up	Agriculture	Vegetation	Swampy	Water	Total	UAcc. (%)	Cerr
Built-up	84	4	0	0	0	88	95.45	0.05
Agriculture	4	77	2	0	0	83	92.77	0.07
Vegetation	1	2	70	5	0	78	89.74	0.10
Swampy	0	1	0	83	0	84	98.81	0.01
Water	0	0	0	0	84	84	100	0
Total	89	84	72	88	84	417	Over All=95.44%	
Pro Acc. (%)	94.38	91.67	97.22	94.32	100	94.38	(K^) =0.94	
Oerror	0.06	0.08	0.03	0.07	0			

Note: UAcc. =User's Accuracies, PAcc. Producer's Accuracies, OAcc. =Overall accuracy, K^ = Kappa Statistics, Cerr= Commission error and Oerror= Omission error

Finally, urban (built-up), swampy and water land use/land cover types had the highest user's accuracy in all classified images. For the 1986, 1998, 2010 and 2017 data, vegetation area had the lowest user's accuracy that is 86.02%, 84.76, 87.39% and 89.74% respectively. For the 1986 classified image, agriculture land has the lower user's accuracy that is 86.06%. All land uses/land cover were found to be more reliable with above 85% of user's accuracy in all four years. For the 1986 classified image, vegetation land cover has the lowest producer's accuracy that is 81.63%.Except vegetation (81.63%), all land use/land cover found to be reliable above 90% of producer's accuracy in all classified images.

In this study, overall kappa coefficients of these classified images of 1986, 1998, 2010 and 2017 were 0.91, 0.93, 0.94 and 0.94, respectively (Eq., 4.6). Therefore, according to Landis, and Koch, 1997) the overall Kappa coefficients of all four years was obtained which was related to as almost perfect (Table 4.2).

5.2 Land use/land cover change detection

The land use/land cover change statistics were calculated from each consecutive pair of LULC maps (1986-1998, 1998-2010 and 2010-2017), and the results of these changes are presented in Table 5.5. This shows the nature of change with respect to each class obtained from a matrix algorithm. Change detection analysis results show a sharp growth of 121.68% in the urban (built-up) class during the 30-year period (1986-2017).Significant differences appear to be related to swampy, vegetation and agriculture land cover classes. Swampy, vegetation cover and agriculture was reduced by 11.38%, 8.81% and 5.52% respectively.

Table 5.6: “From-to” LULC change detection statistics for 1986-2017 for study area in Km^2.

		1986-1998		1998-2010		2010-2017		1986-2017	
S.No	LULC type	Area (Km^2)	%	Area (Km^2)	%	Area (Km^2)	%	Area (Km^2)	%
1	Urban(built-up)	1.2	3.60	18.37	53.23	20.96	39.64	40.53	121.68
2	Agriculture	26.21	13.91	-15.64	7.33	-20.88	-10.58	-10.31	-5.52
3	Vegetation	-42.39	-21.69	8.08	5.28	17.09	10.61	-17.22	-8.81
4	Swampy	17.16	31.95	-8.42	-11.88	-14.85	-23.78	-6.11	-11.38
5	Water	-2.99	-3.29	-1.6	-1.82	-2.82	-3.27	-7.41	-8.16

Land use land cover change between 1986 and 1998

During the first period (1986-1998) the land use land cover change was characterized by abrupt rise in urban (built-up) area by approximately 3.60%, agriculture land increased by 13.91% and swampy area by 31.95%. On the other hand, vegetation cover and water bodies decreased by 3.29% and 21.69% respectively (Figure 5.5).

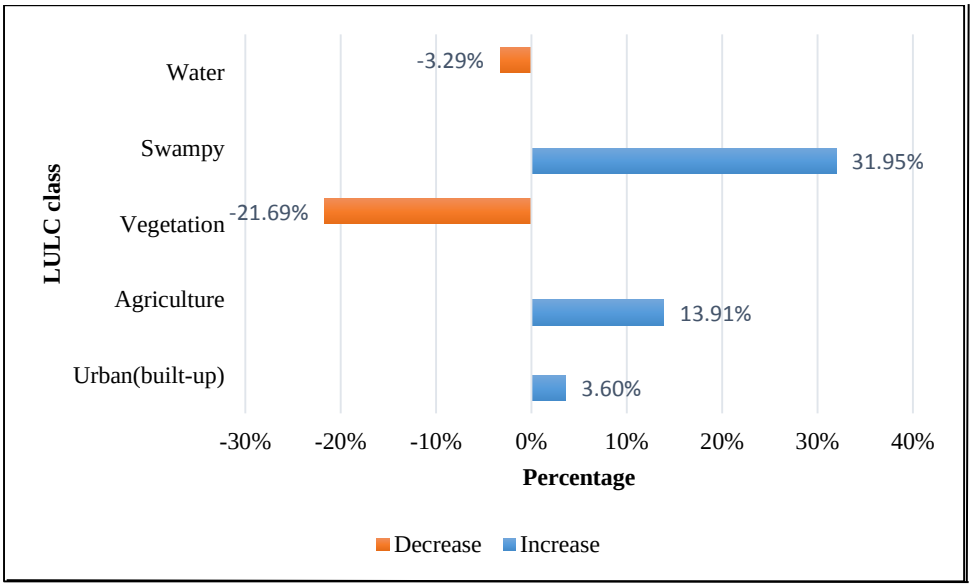

Figure 5.5: LULC change in the study area from 1986 to 1998 in percentage.

Land use land cover change between 1998 and 2010

In the second period (1998-2010), urban (built-up) increased sharply by approximately 53.23%. Agriculture land decreased by 7.33% from the first period and vegetation cover showed an opposite trend in this period as compared to the first period which increased by 5.28%. For swampy area the declining trend reduced sharply decreasing from the first period by 11.88%. Whereas, water body slightly decreased from the first period by 1.8 %(Figure 5.6).

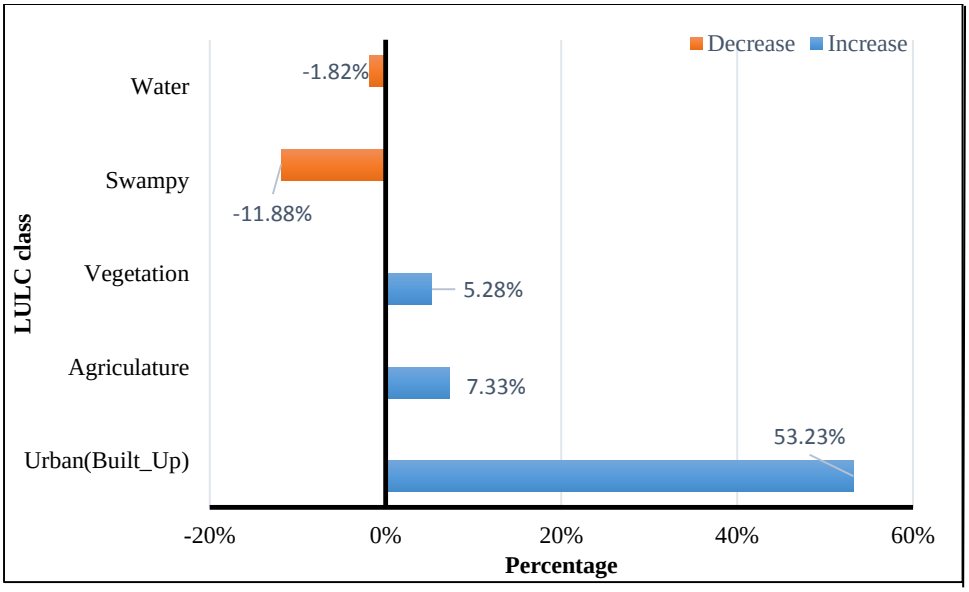

Figure 5.6: LULC change in the study area from 1998 to 2010 in percentage.

Land use land cover change between 2010 and 2017

In the 3rd period (2010-2017), urban (built-up) increased by approximately 39.64% from the second period. But vegetation cover increased by 10.61% from the second period. swampy and water bodies showed an opposite trend in this period as compared to the first period with area declining by 23.78% and 3.27% respectively. Agriculture land decaling trend reduced by 8.86% from the second period (Figure 5.7).

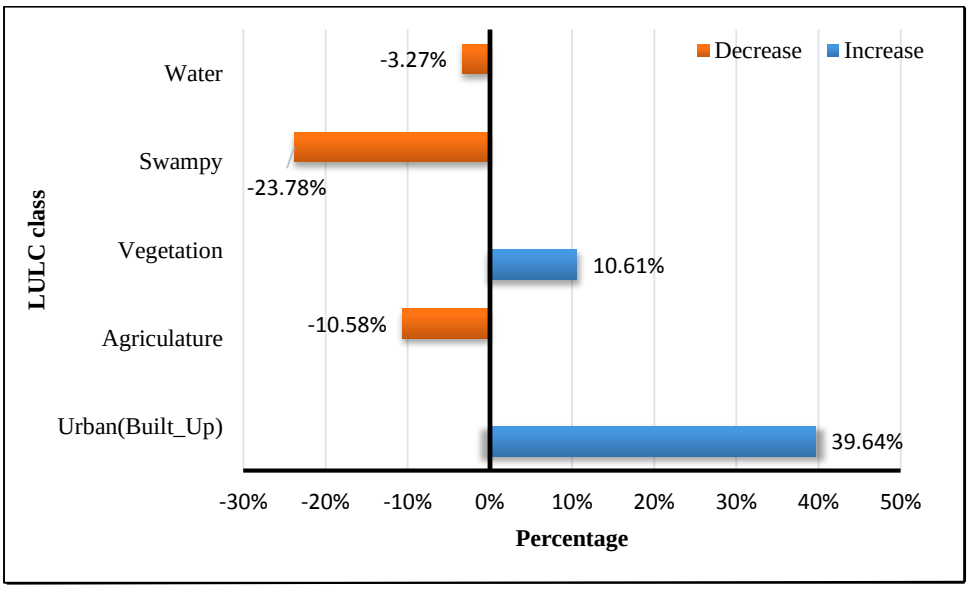

Figure 5.7: LULC change in the study area from 2010 to 2017 in percentage.

Land use land cover change between 1986 and 2017

This period (1986-2017) was in fact the overall change from the first, second and third period. There was extreme increment in urban (built-up) land by approximately increased by 121.68%. But vegetation, swampy, water body and agriculture land were reduced by 8.81%, 11.38%, 8.16% and 5.52% respectively (Figure 5.8).

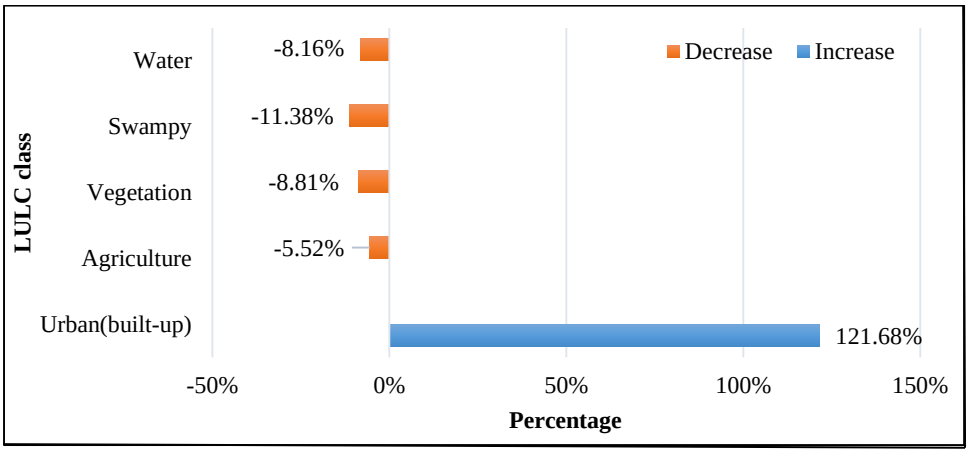

Figure 5.8: LULC change in the study area from 1986 to 2017 in percentage.

5.3 Land use land cover indices

5.3.1 Normalization Difference Built-up Index (NDBI)

NDBI maps (Figure 5.9) revealed an opposite pattern to the NDVI maps in the sense that vegetation cover, water bodies and other swampy area with high NDVI values and received low NDBI values. Likewise, urban (built-up) area with low NDVI received high NDBI value. The lowest NDBI was computed from water bodies while the highest values were possessed by agriculture land and urban (built-up) area. In general, urban(built-up) areas have higher reflectance in relation to SWIR band and it was thus expected to have higher NDBI but some studies show that reflectance for certain types of vegetation cover increases as water content decreases (Cibula et al., 1992; Gao, 1996). The drier vegetation can even have higher reflectance to SWIR resulting in higher NDBI (Gao, 1996). It is observed that higher NDBI values correspond to urban (built-up) areas and agriculture area in the central and west part of the study area, while lower values were observed in water bodies, swampy and vegetation area. NDBI values are in the range of -0.72 to 0.5.52 in 1986,-0.88 to 0.32 in 1998, -0.77 to 0.22 in 2010 and -0.86 to 0.47 in 2017(Eq.4.8).

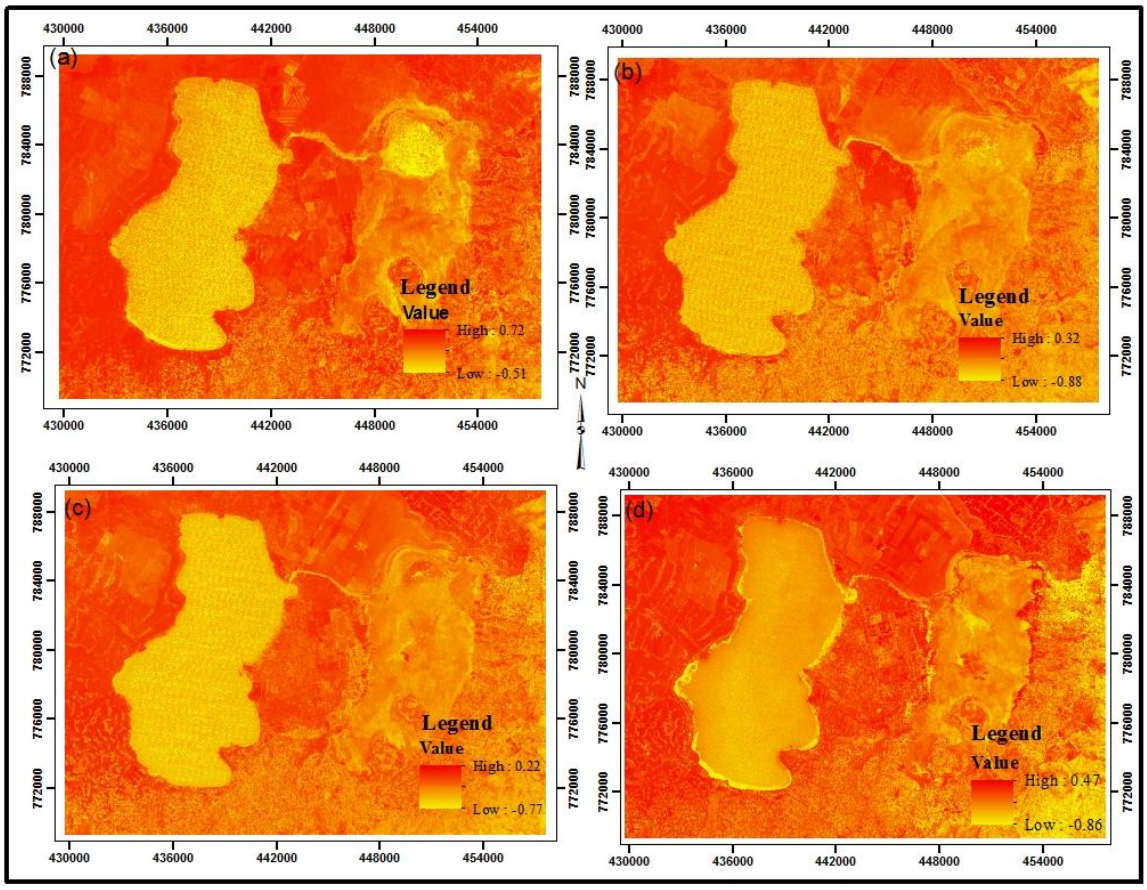

Figure 5.9: Spatial distribution of NDBI for the years (a) 1986, (b) 1998, (C) 2010 and (d) 2017.

5.3.2 Normalization Difference Vegetation Index (NDVI)

Figure 5.10 shows the spatial distribution of NDVI in the study area. It is observed that higher NDBI values correspond to vegetation cover and swampy areas in the northeast and north south part of the study area edges and also the edge of Hawassa Lake, which represent the vegetation cover and swampy area. Low NDVI values can be observed concentrated primarily in the urban (built-up) and agriculture region which corresponds to the urban (built-up) area.

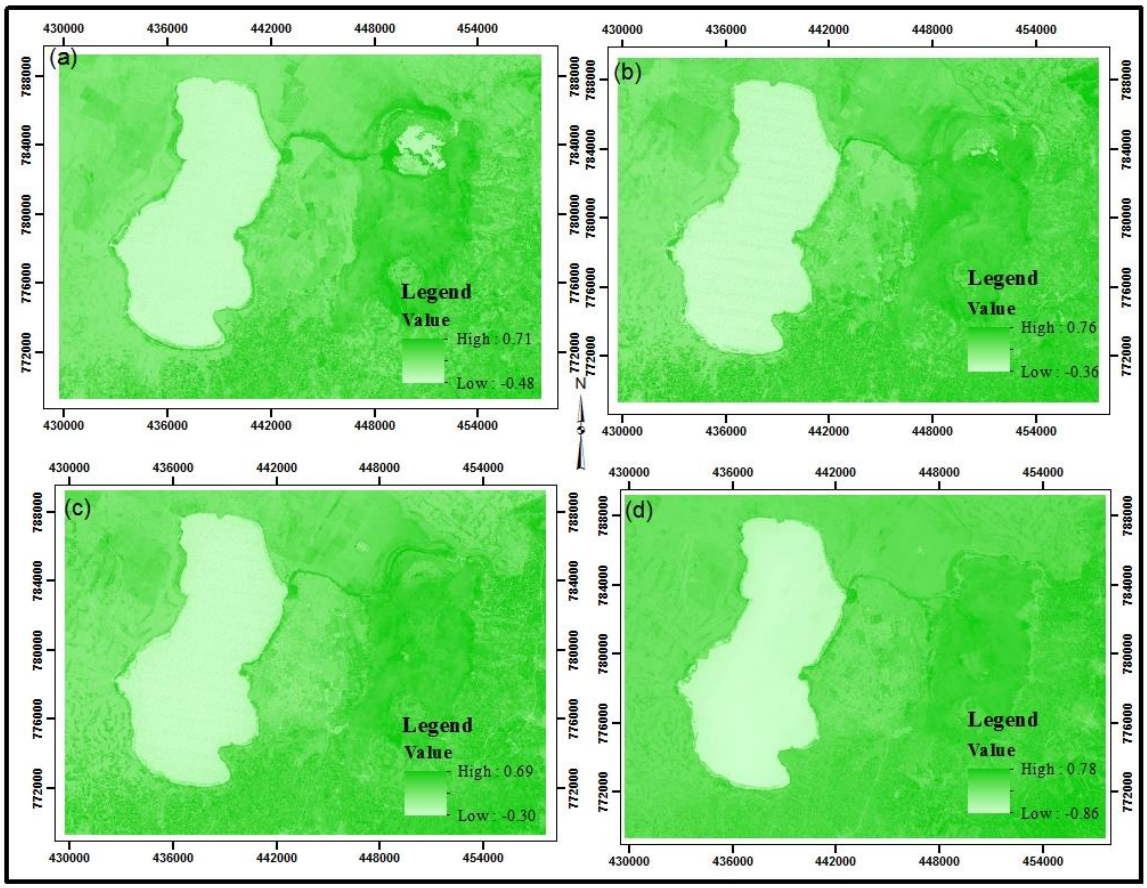

Figure 5.10: Spatial distribution of NDVI for the years (a) 1986, (b) 1998, (c) 2010 and (d) 2017.

Figure 5.11 shows the bar chart of mean NDVI values for each land use land cover class. The land use land cover class with the highest mean NDVI value was vegetation cover and swampy area with NDVI value ranging from 0.30 to 0.51 for 1986 to 2017.The other land use land cover class with medium NDVI value was agriculture land from 0.11 to 0.25 and NDVI value for the urban (built-up) area was ranges from 0.13 to 0.30.Urban (built-up) and agriculture land class showed medium NDVI values due to the dominance of vegetated cover. The lowest mean NDVI was for water ranged from -0.19 to -0.69(Eq., 4.7).

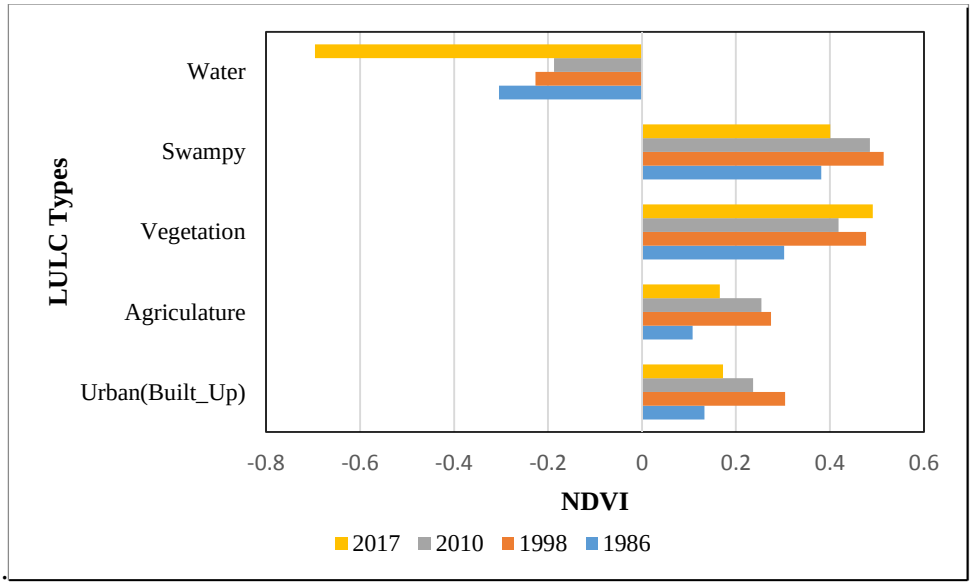

Figure 5.11: Mean NDVI values for each land use land cover class in 1986, 1998, 2010 and 2017.

5.3.3 Normalized Difference Water Index (NDWI)

Figure 5.12 shows the spatial distribution of NDWI in the study area. Most of the land use land cover classes received low NDWI value. As expected, water body got the highest NDWI value in all four years whereas agriculture land got the lowest NDWI. Regarding swampy and vegetation land cover class, though the mean NDWI value is highly negative. It can also be observed that the range of NDWI value in 1986 the range from -0.77 to 0.77,in 1998 the range from -0.50 to 0.95,in 2010 the range from -0.58 to 0.44 and in 2017 the range from -0.67 to 0.90.

Figure 5.13 was a bar chart showing mean NDWI value within each land use land cover class for the years 1986, 1998, 2010 and 2017. As observed, water body was the only land use land cover class with positive NDWI value ranging from 0.30 to 0.78. Urban (built-up), vegetation cover, swampy and agriculture land demonstrated highly negative NDWI value (-0.17 to -0.66) (Eq., 4.9).

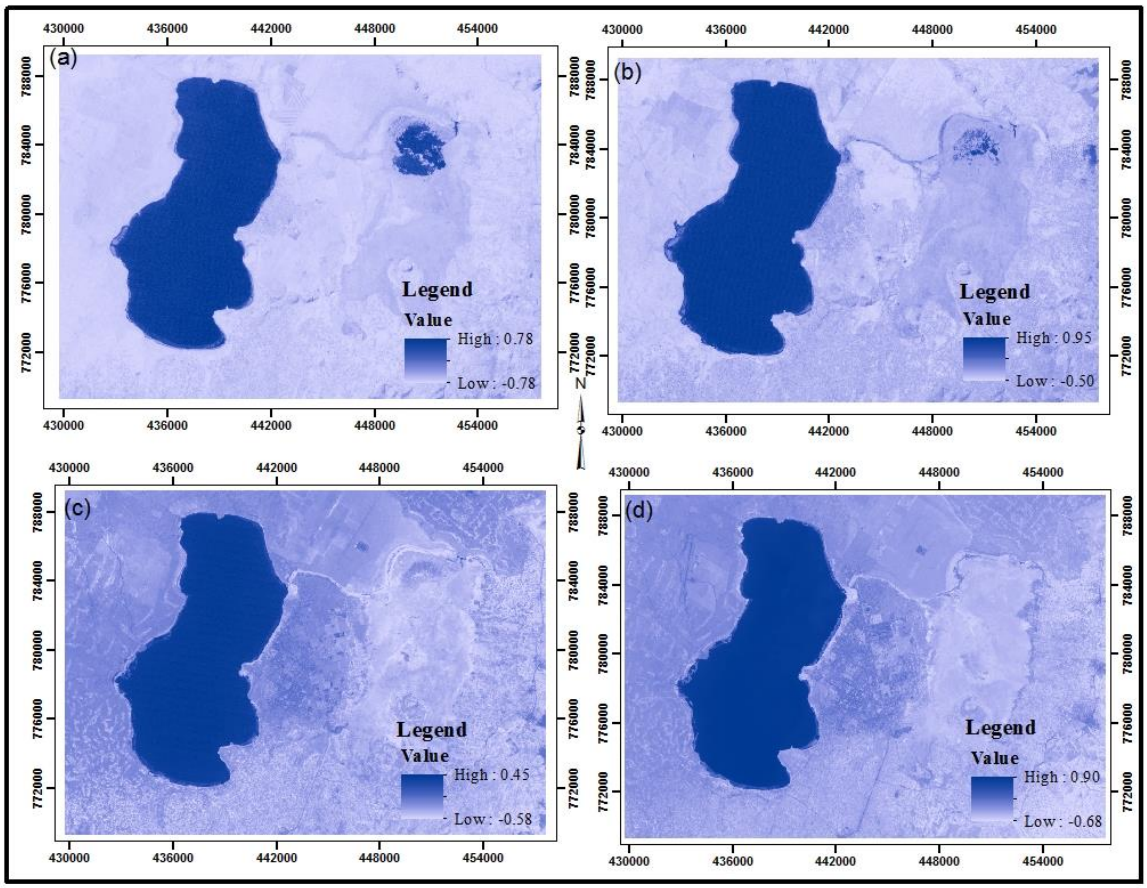

Figure 5.12: Spatial distribution of NDWI for the years (a) 1986, (b) 1998, (c) 2010 and (d) 2017.

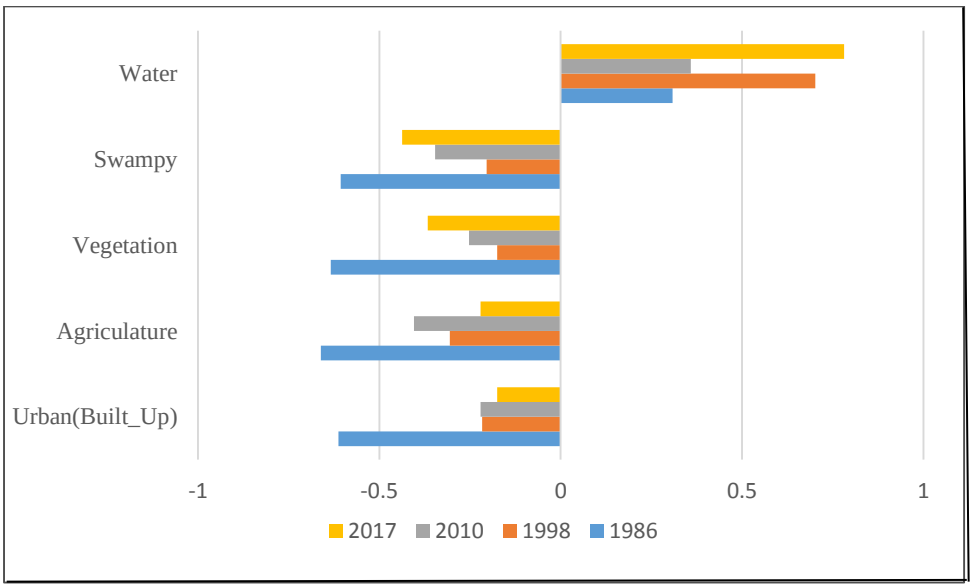

Figure 5.13: Mean NDWI within each Land Use class in 1986, 1998, 2010 and 2017.

5.4 Spatial pattern of land surface temperature

Land surface temperature maps of the study area in 1986, 1998, 2010 and 2017 are presented in Figure 5.14, 5.15, 5.16 and 5.17 respectively. The computed values of the land surface temperature are ranged from 10.92 ^{0}C to 36.83 ^{0}C, with the mean values of, 23.88 ^{0}C in 1986, from 12.83 ^{0}C to 36.04 ^{0}C, with the mean value of 24.44 ^{0}C in 1998, from 14.25 ^{0}C to 38.38 ^{0}C, with the mean value of 26.32 ^{0}C in 2010 and from 15.39 ^{0}C to 39.67 ^{0}C, with the mean value of 27.53 ^{0}C in 2017.The mean temperature increased by 0.56 ^{0}C from 1986 to 1998, 1.88 ^{0}C from 1998 to 2010, 1.21 ^{0}C from 2010 to 2017. Besides, the mean land surface temperature increased sharply by 3.65 ^{0}C from 1986 to 2017.However, there was a gradual increase in the minimum temperature in the subsequent years. The sudden increase in the maximum temperature during 1986 to 2017 can be reasonable, as some days of the year in the past can be hotter despite of the influence of urban warming phenomenon caused by urban expansion over time. The LST pattern is strongly correlated with LULC distribution. A large proportion of very high LST value (dark red color) is mainly distributed on the bare soil and roof top of the building. Thus high LST represented by red patch for agriculture area and also high LST represented by heavy yellow and red color for urban (built-up) area. Therefore, the high LST area (heavy yellow and red color) appears as a big island surrounded by low LST regions (represented in blue). Therefore, low temperature represented by blue tone for water bodies, swampy and vegetation land use land cover types.

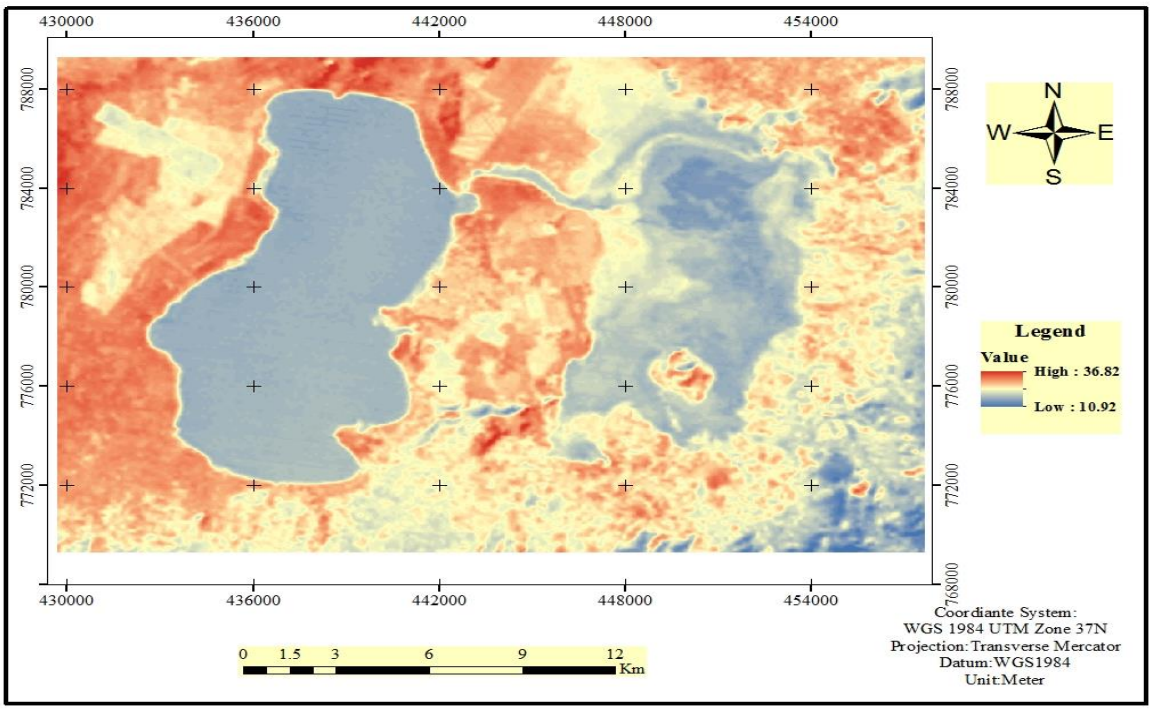

Figure 5.14: Spatial pattern of land surface temperature map in 1986.

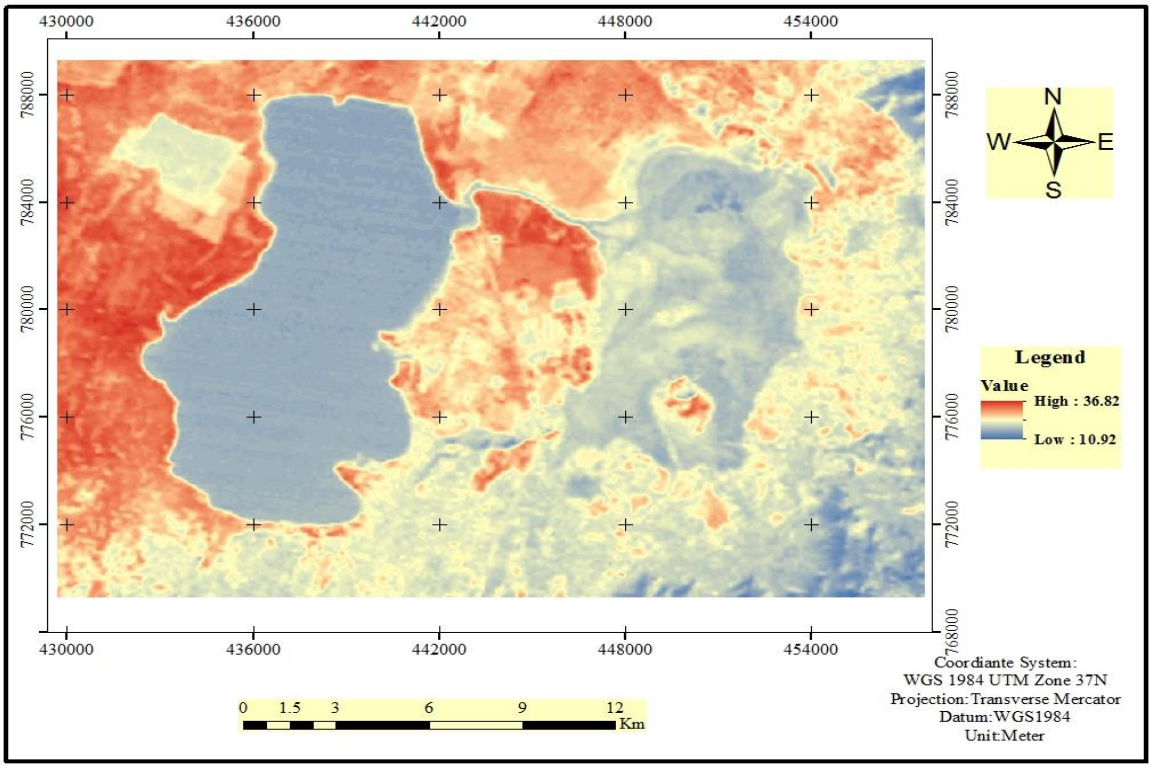

Figure 5.15: Spatial pattern land surface temperature map in 1998.

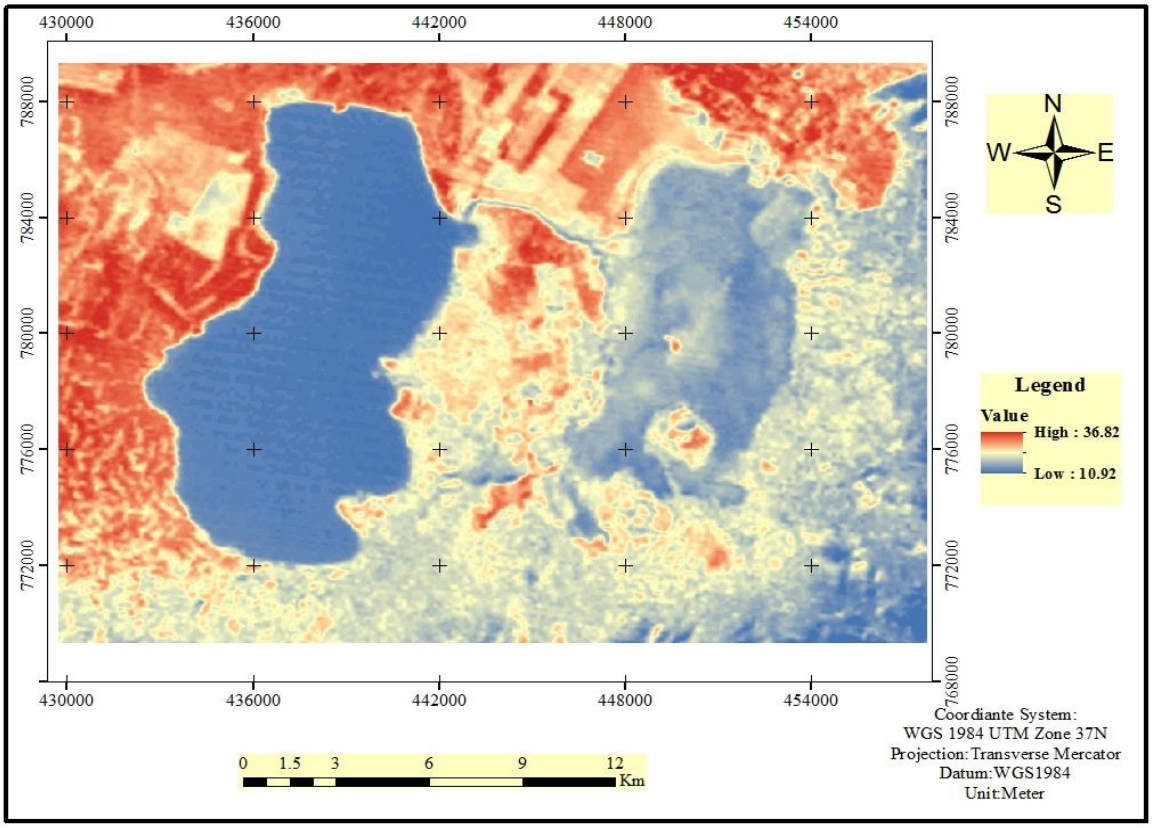

Figure 5.16: Spatial pattern of land surface temperature map in 2010.

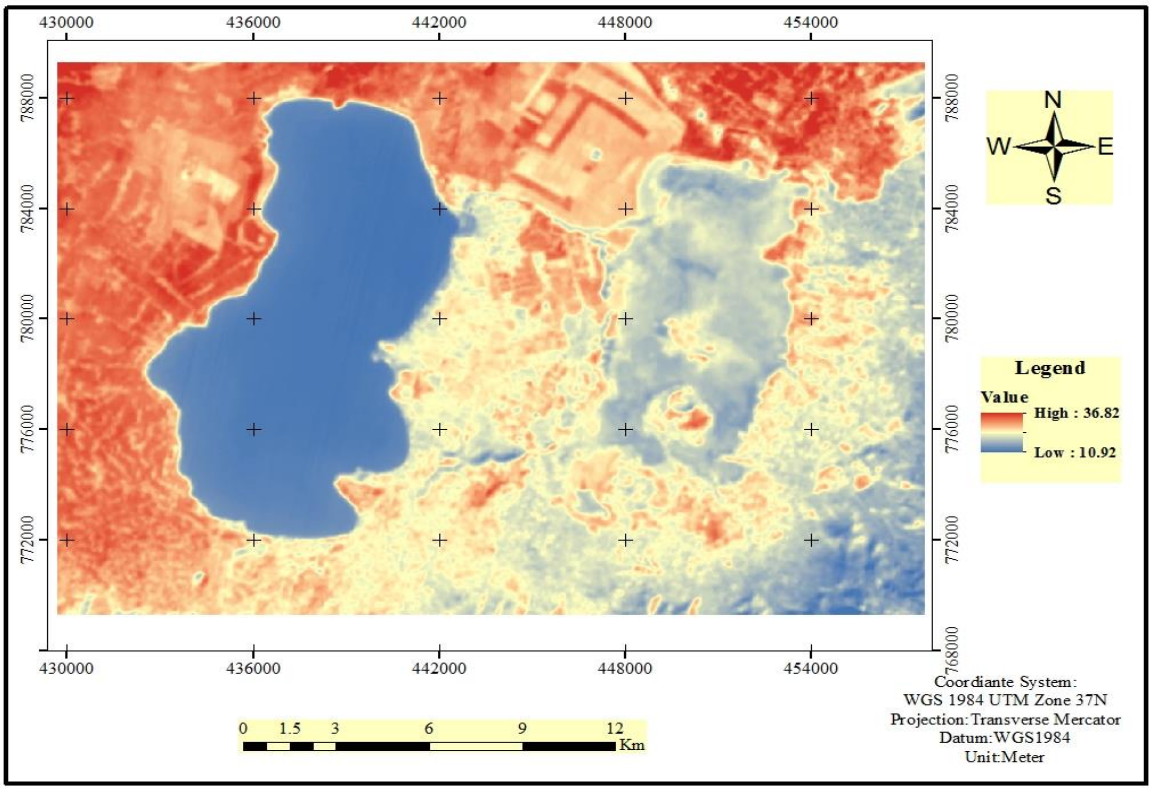

Figure 5.17: Spatial pattern of land surface temperature map in 2017.

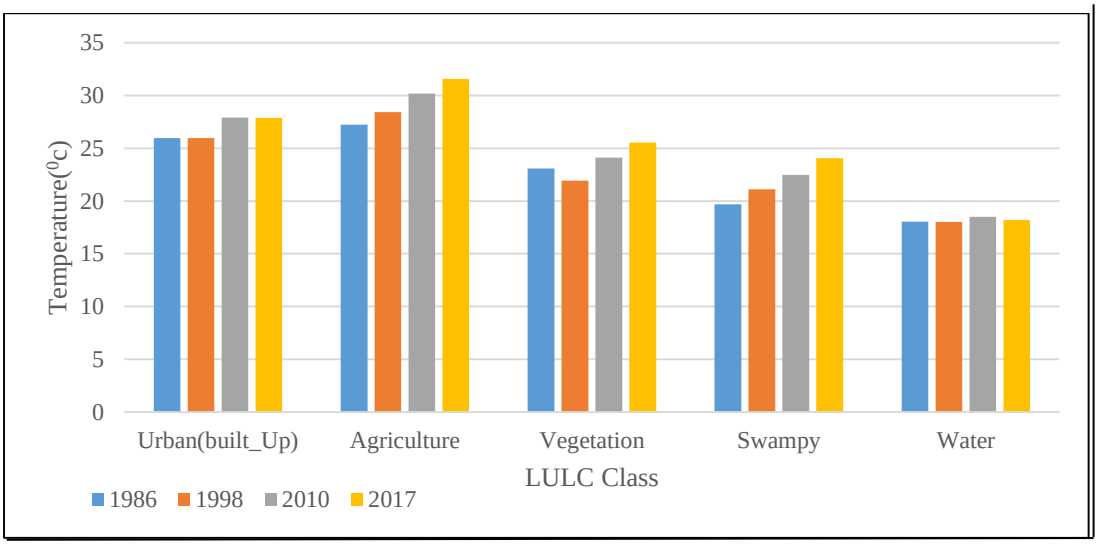

Figure 5.18: Mean land surface temperature for each LULC class in different years.

Figure 5.18 shows the mean land surface temperature within each land use land cover class in the study area. Water bodies and swampy land cover types are characterized by the minimum mean land surface temperature values(for water body 18.06 ^{0}C in 1986, 18.01^{0}C in 1998,18.51^{0}C in 2010 and 18.19 ^{0}C in 2017 and for swampy 20.62 ^{0}C in 1986, 21.92 ^{0}C in 1998,22.47 ^{0}C in 2010 and 24.06 ^{0}C in 2017).Followed by swampy and water bodies cover

types, vegetation were the smallest mean land surface temperature compared with the three years period (23.52 ^{0}C in 1986, 21.11 ^{0}C in 1998,22.47 ^{0}C in 2010 and 25.55 ^{0}C in 2017).Agriculture land got to the maximum mean land surface temperature values in all four years (27.11 ^{0}C in 1986, 28.4 ^{0}C in 1998, 30.17 ^{0}C in 2010 and 31.58 ^{0}C in 2017). After agriculture land, urban (built-up) area got the highest mean land surface temperature values (26.43 ^{0}C in 1986, 25.95 ^{0}C in 1998, and 27.89 ^{0}C in 2010 and 27.88 ^{0}C in 2017).

In this way, water body and swampy areas received low mean land surface temperature values, vegetation area received medium mean land surface temperature, and urban (built-up) and agriculture received high values of mean land surface temperature. The comparison of mean land surface temperature for urban (built-up) land type from 1986 to 2017, the maximum temperature was observed in 2017 relative to 1986. This justifies the urban warming effect increasing in the study area due to urban explanation over time.

5.5 Relationship between land surface temperature and LULC indices

The land use/land cover indices, as mentioned in section 4.5, were derived to assess the relationship between LST and land use/land cover indices. LST and NDVI, NDBI and NDWI indices were used for this purpose. The result shows that decreasing surface transpiration through the reduction green cover and increasing impervious surfaces modified thermal behavior and was essential to the reduced value of NDVI and increased NDBI. This pattern can be clearly seen in Tables 5.7 and 5.8, showing the correlation between the land use land cover indices and LST. Therefore, the sign of the correlation coefficient determines whether the correlation positive or negative. The magnitude of the correlation determines the strength of the correlation. Correlation is an effect size and so we can verbally describe the strength of the correlation using the guide that (Evans, 1996) suggest for the absolute value of r: 0.00-0.19: “very week”, 0.20-0.39:”weak”, 0.40-0.59:”moderate”, 0.60-0.79:”strong” and 0.80-1.00:”very strong”. According to Evans (1996), the results revealed that the correlation between LST and NDBI was significantly strong positive correlation. The value of correlation between LST and NDBI was 0.89, 0.90, 0.86 and 0.85 in 1986, 1998, 2010 and 2017 respectively. Therefore, urban (built-up) areas and agricultural land cover can reinforce urban heat effects and increase LST in and around Hawassa Town (Figure 5.19). Whereas, NDVI value was highly negatively correlated with LST, indicating the impact of green cover on LST is negative, in which the more green areas, the weaker LST (Figure 5.20).The value of the correlation between LST and NDVI was -0.86,-0.82,-0.74 and -0.76 in 1986, 1998, 2010 and 2017, respectively. Thus, in 1986,1998, 2010 and 2017 the correlation between

LST and NDVI is strong correlation. The NDWI was negatively correlated with the LST for 1986, 1998 and 2010 strong correlation with LST but in 2017 moderately correlated with LST. It was interesting to note that the high negative correlation between NDVI and NDBI in the four years could be explained by the action of establishing urban settlements planned with green space and agriculture area use agroforestry mechanize.

Table 5.7: Correlations between LST, Land use/land cover indices in 1986 and 1998.

	December 24,1986				December 08,1998			
	LST	NDBI	NDVI	NDWI	LST	NDBI	NDVI	NDWI
LST	1	0.89	-0.86	-0.62	1	0.90	-0.82	-0.61
NDBI	0.89	1	-0.94	-0.79	0.90	1	-0.90	-0.79
NDVI	-0.86	-0.94	1	-0.86	-0.82	-0.90	1	-0.85
NDWI	-0.62	-0.79	-0.85	1	-0.61	-0.79	-0.85	1

Table 5.8: Correlations between LST, Land use/land cover indices in 2010 and 2017.

	December 09,2010				December 28,2017			
	LST	NDBI	NDVI	NDWI	LST	NDBI	NDVI	NDWI
LST	1	0.86	-0.74	-0.61	1	0.85	-0.76	-0.58
NDBI	0.86	1	-0.87	-0.61	0.85	1	-0.92	-0.21
NDVI	-0.74	-0.87	1	-0.98	-0.76	-0.92	1	-0.99
NDWI	-0.61	-0.61	-0.98	1	-0.58	-0.21	-0.99	1

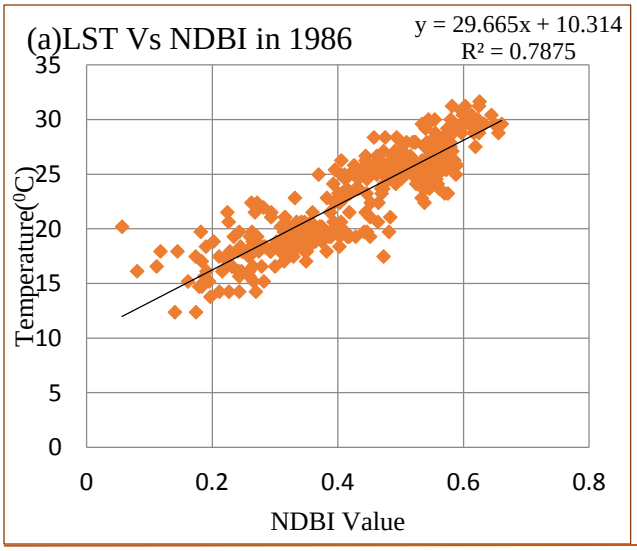

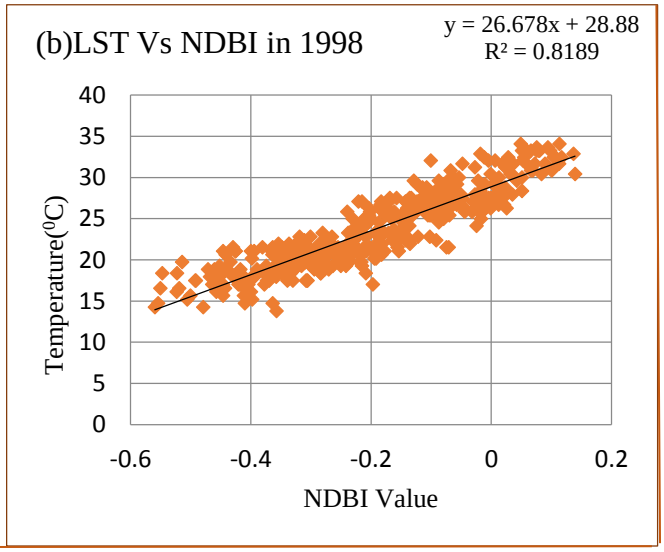

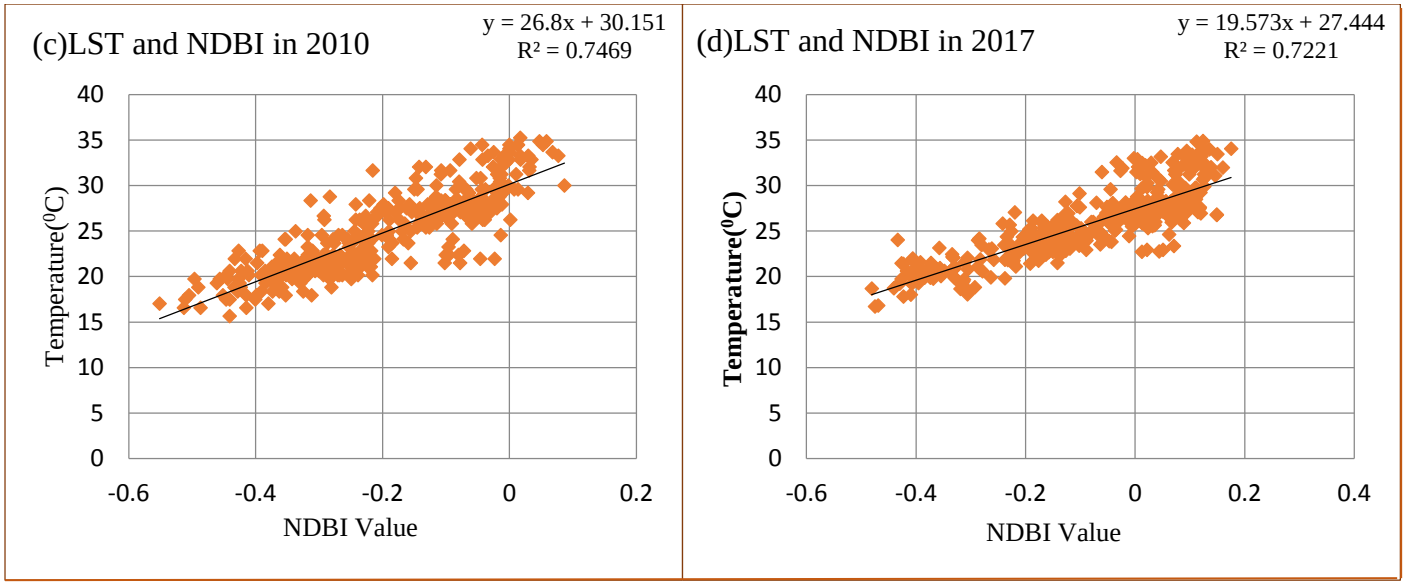

Figure 5.19: Correlation between NDBI and LST for the years (a) 1986, (b) 1998, (c) 2010 and (d) 2017.

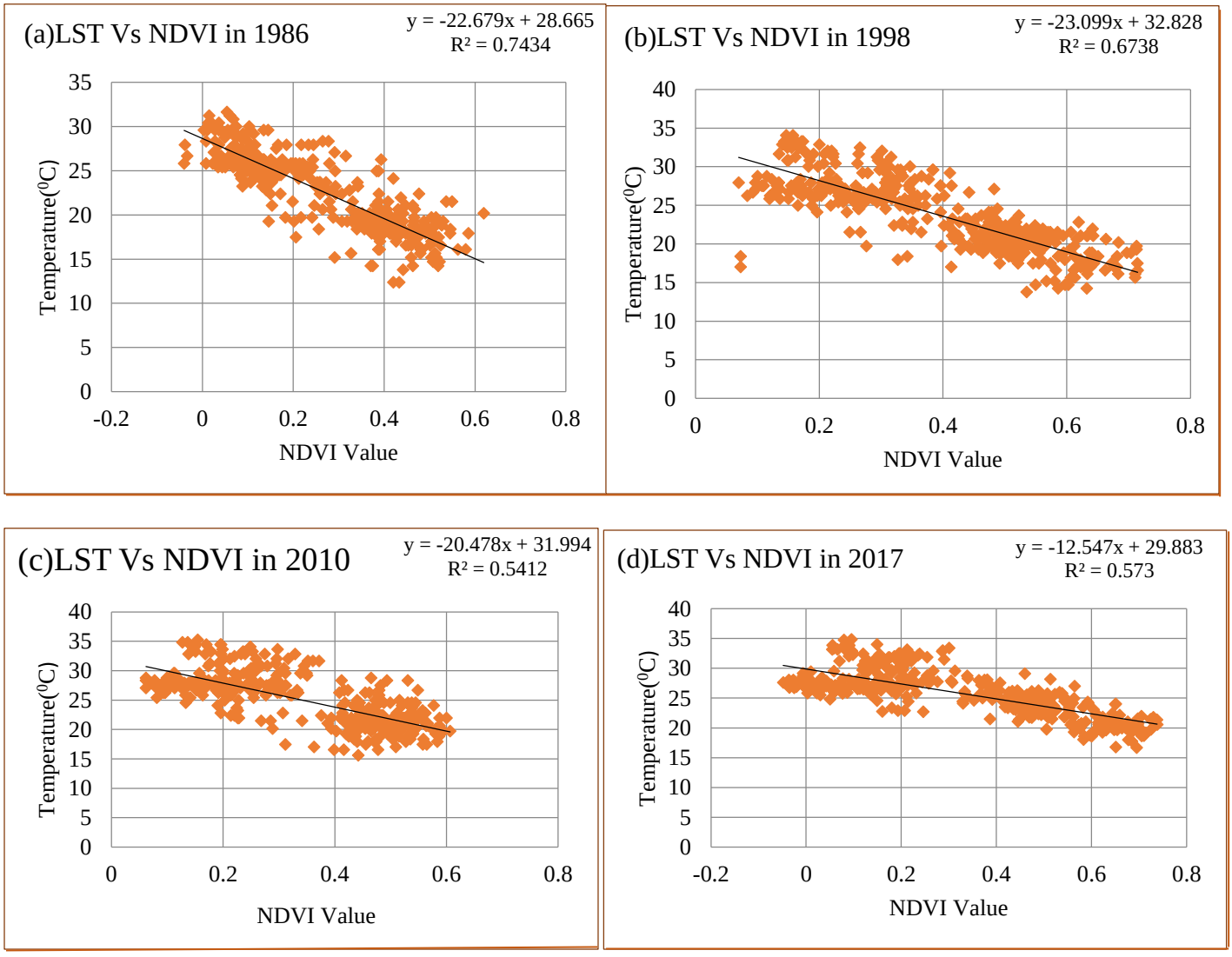

Figure 5.20: Correlation between NDVI and LST for the years (a) 1986, (b) 1998, (c) 2010 and (d) 2017.

5.5.1 Linear Regression of LST and Land use/land cover class

Regression models were further developed for each land use/land cover class to understand its relationship to land surface temperature systematically. Table 5.9 and 5.10 shows regression models for each land use/land cover class in the study area between the period in 1986 and 2017.

Table 5.9: Pearson's correlation between LST and NDBI by each LULC class with confidence level 95%

	LST Vs. NDBI 1986				LST Vs. NDBI 2017			
LULC	R^2	Regression Equation	Cor.	RMSE	R^2	Regression Equation	Cor.	RMSE
UB	0.74	LST=10*NDBI+20.88	0.86	0.70	0.44	LST=10.56*NDBI+27.01	0.66	1.47
AL	0.50	LST=46.49*NDBI+0.70	0.71	1.70	0.28	LST=21.67*NDBI+29.78	0.53	1.80
VC	0.04	LST=-4.31*NDBI+16.78	-0.21	1.47	0.11	LST=4.14*NDBI+21.13	0.33	2.09
S	0.21	LST=13.96*NDBI+15.16	0.45	1.27	0.16	LST=7.71*NDBI+24.89	0.40	0.79
WB	0.01	LST= -0.83*NDBI+18.37	-0.10	0.42	0.13	LST= -3.68*NDBI+17.17	-0.36	0.33

Note: Cor. =Correlation UB=Urban (built-up), AL=Agriculture land, VC=Vegetation Cover, S=Swampy and WB=Water bodies

Table 5.10: Pearson's correlation between LST and NDVI by each LULC class with confidence level 95%.

	LST Vs. NDVI 1986				LST Vs. NDVI 2017			
LULC	R^2	Regression Equation	Cor.	RMSE	R^2	Regression Equation	Cor.	RMSE
UB	0.21	LST= -5.99*NDVI+26.57	-0.46	0.70	0.03	LST= -3.15*NDVI+28.13	-0.17	1.59
AL	0.22	LST=-16.16*NDVI+28.86	-0.47	0.22	0.44	LST= -21.83*NDVI+34.93	-0.66	1.56
VC	0.28	LST= -17.08*NDVI+26.65	-0.56	1.65	0.57	LST=-28.67*NDVI+39.18	-0.75	2.02
S	0.29	LST= -9.04*NDVI+22.71	-0.55	0.10	0.27	LST= -13.04*NDVI+30.53	-0.52	1.18
WB	0.10	LST= -5.73*NDVI+16.26	-0.32	0.40	0.10	LST= -4*NDVI+15.02	-0.32	0.34

Note: Cor. =Correlation UB=Urban (built-up), AL=Agriculture land, VC=Vegetation Cover, S=Swampy and WB=Water bodies

Results showed that the NDBI index showed a positive correlation with all land use/land cover types except for water bodies and vegetation cover in 1986 and 2017, which had negative or almost no correlation with LST.

In 1986, the highest positive coefficient of the regression function was found in the urban (built-up) (0.66). Also, the correlation between urban (built-up) and land surface temperature is strong correlation (Table 5.9).

In 2017, the highest positive coefficient of the regression function was found in the urban (built-up) (0.86). The strength of the correlation between urban (built-up) and land surface temperature is strong correlation (Table 5.9).

However, the correlation between LST and NDVI were all negative in both 1986 and 2017.In 1986, the lowest negative correlation was found on water body class due to the high coverage of the Lack of Hawassa in the study region. The highest negative coefficient of the regression function was found to be in vegetation cover (-0.56) and the second highest land use/land cover class is the swampy area (-0.55) (Table 5.10).

In 2017, the lowest negative correlation was found on urban (built-up) land use/land cover. The highest negative coefficient of the regression function was found to be in vegetation cover (-0.75) and the second highest land use land cover class is the agriculture land (-0.66) (Table 5.10).

Results of this analysis are consistence with other studies discussing the relationship between LST and NDVI (Wilson et al., 2003 and Weng et al., 2004).This indicated that by increasing NDVI, the LST of both vegetation and agriculture land decreases more quickly than that of urban (built-up) and water land cover.

In general, the correlation coefficient between LST and land surface indices for the whole study area showed a higher correlation than in the case of using indices as indicators for LST according to each land use/land cover types. However, moderate relationship obtained for each land use/land cover by surface indices and LST can provide important information for preliminary studies; for example, they can be simply used as proxies for temperature and for better planning by policy makers in large areas.

5.6 Surface temperature intensity and its relation to LULC types

To assess the impact of land use/land cover change on the UHI effect, the hotspot pattern change was linked to land use/land cover change through time. This method gives a better demonstration of the UHI effect, rather than focusing only on the high or low land surface temperature absolute values separately.

According to Goswami et al., (2013) Getis-Ord Gi* statistics was applied to the LST dataset to detect the presence of hot or cold spots over the study area. This is considered to be an effective approach to visualize the effect of urban heat island. By this method, we are concerned with the thermal pattern rather than the absolute value of mean surface temperature. It should also be noted that the identification of hot or cold spots by this method does not necessarily imply the mean surface temperature being high or low.

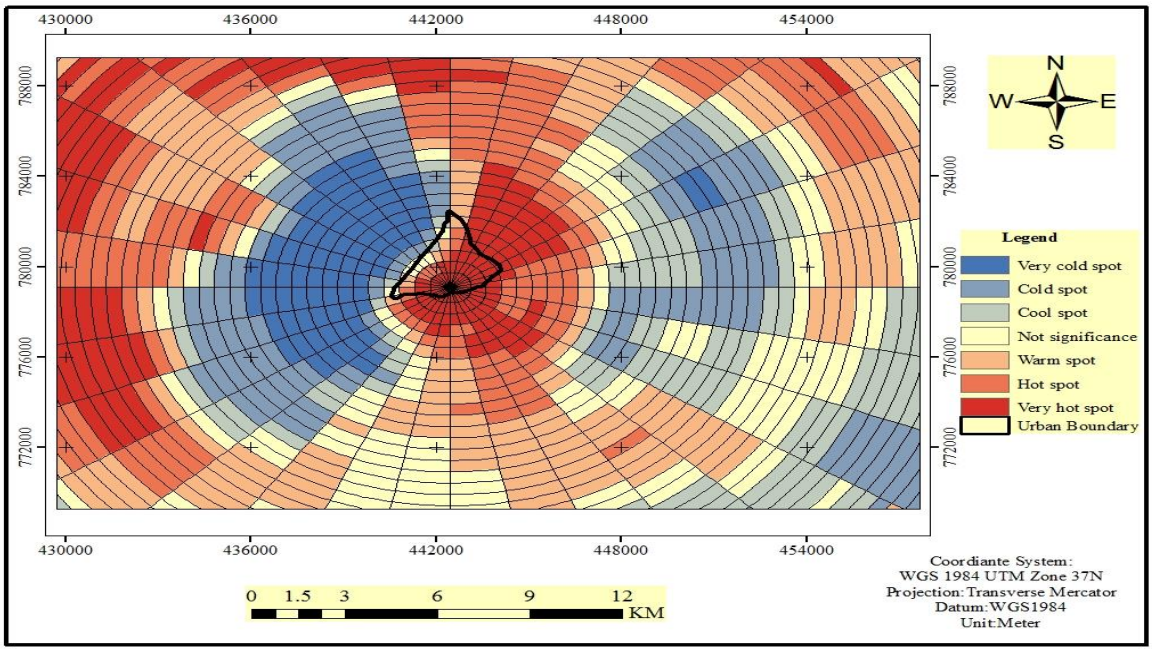

Figure 5.21: Spatial pattern of surface heat intensity shown in terms of Gi*Z_{score} in 1986.

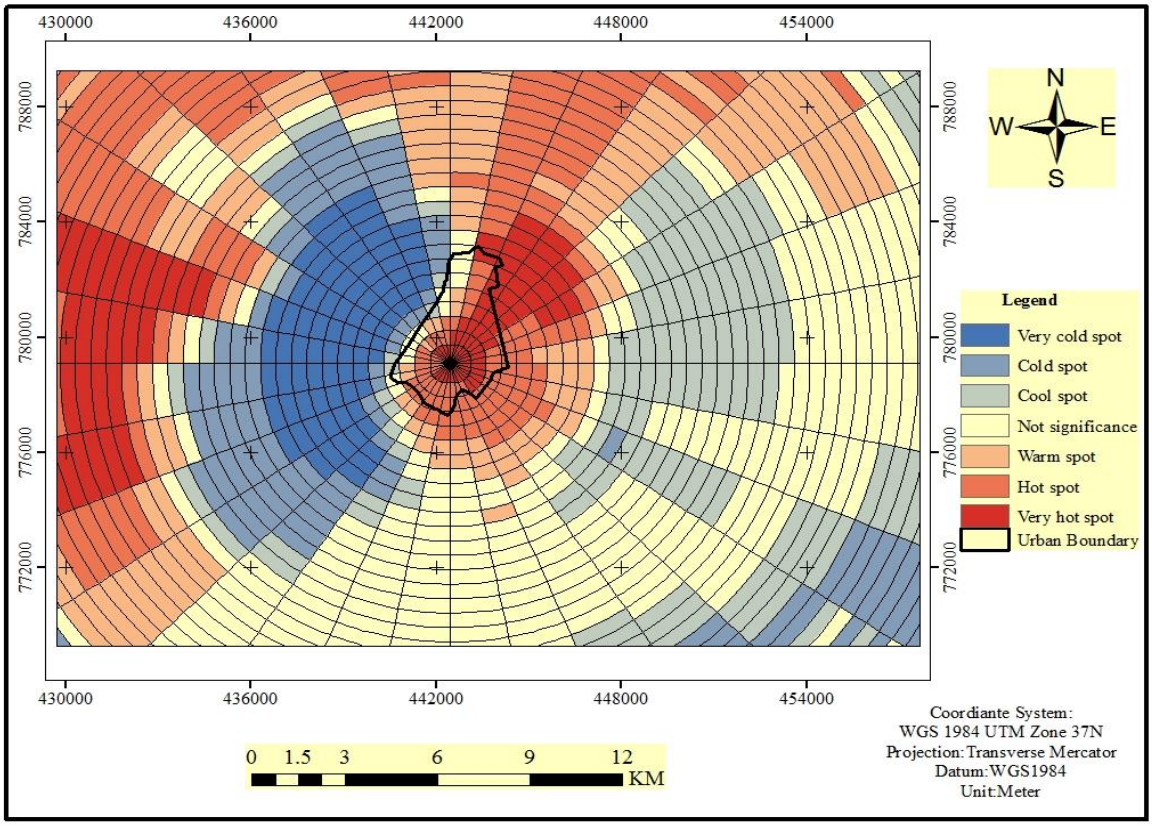

Figure 5.22: Spatial pattern of surface heat intensity shown in terms of Gi*Z_{score} in 1998.

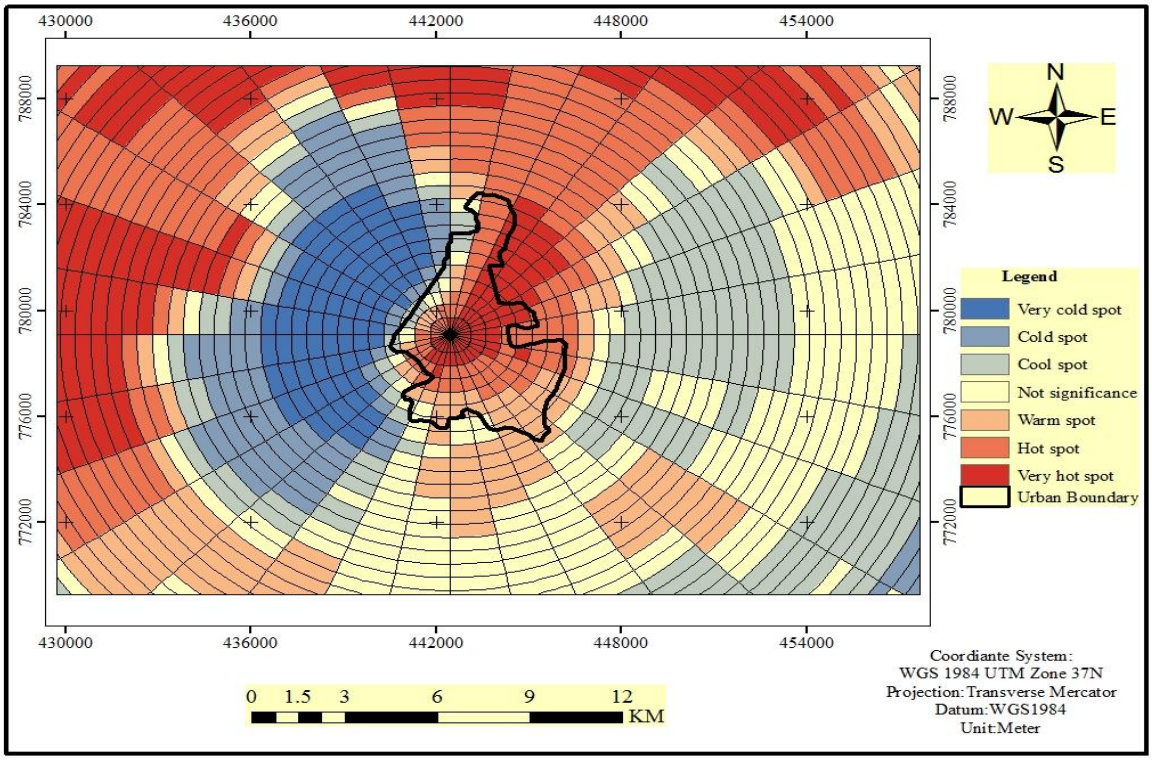

Figure 5.23: Spatial pattern of surface heat intensity shown in terms of Gi^*Z_{score} in 2010.

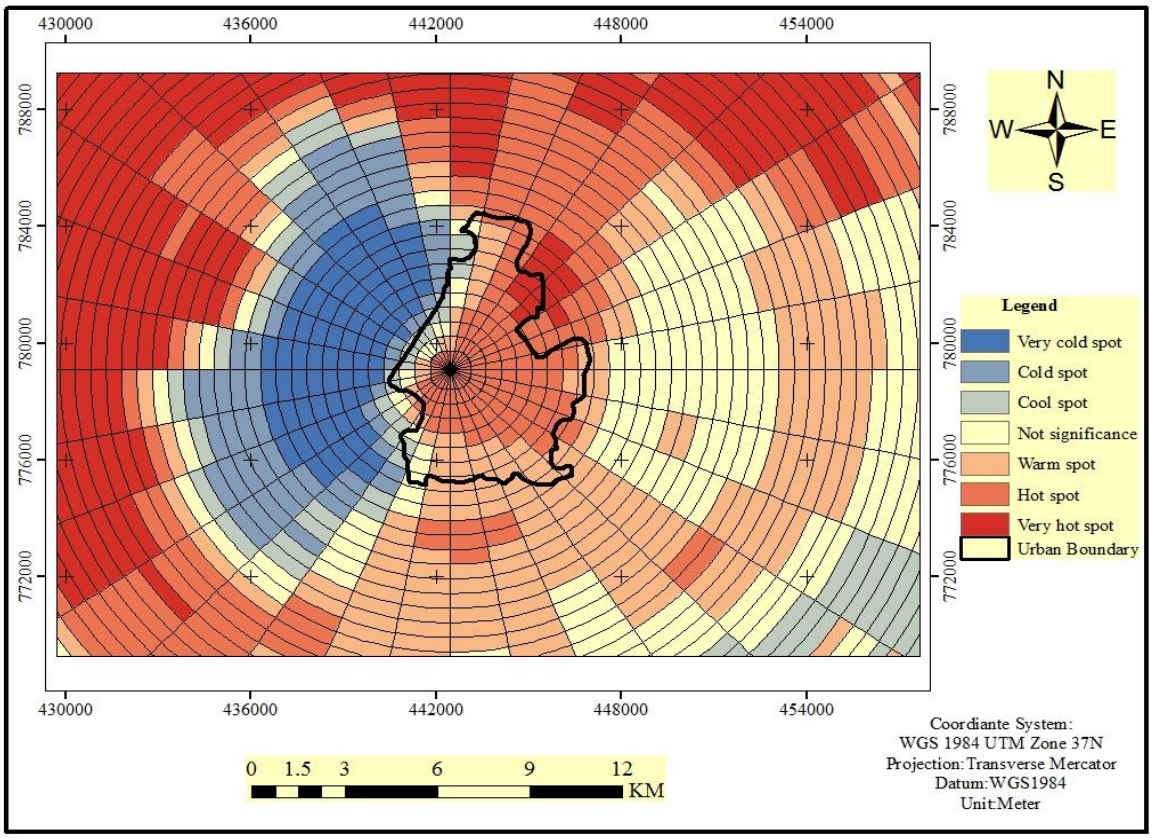

Figure 5.24: Spatial pattern of surface heat intensity shown in terms of Gi^*Z_{score} in 2017.

From the statistics results, the land surface temperature pattern was divided into seven categories: very hot spot, hot spot, warm spot, not statistically significance, cool spot, cold spot and very cold spot. In the final statistics of the hot spots and cold spots in our research, values at 95% confidence level were taken.

The maps for the year from 1986 to 2017 the urban expansion was rapid the intensity of thermal aggregation expanded spatial with the city and primarily show heat island in the urban (built-up) area. High thermal aggregation outside urban (built-up) areas was due to predominance of agriculture land covered by bare soil. There was a formation of big heat island covering almost the whole urban (built-up) and agriculture land in the time periods 1986, 1998, 2010 and 2017 are showed in Figure 5.21, 5.22, 5.23 and 5.24. In 1986, 1998 and 2010 water bodies, swampy and vegetation land use land covers was covered by cold region but in 2017 the swampy area change into not statistically significance. The cold region was observed in the areas of high vegetation cover such as forest, grassland and shrubs. This justifies the importance of vegetation cover, swampy and water bodies in minimizing the urban heat island effect and urban (built-up) and agriculture maximize the urban heat island effect of the study area.

Table 5.11: Summery of Surface Heat Intensity (SHIn) calculated using Hotspot analysis.

Summary of Surface Heat Intensity(SHIn) calculated using hotspot analysis				
No	Years	Mean temperature in hotspot Area	Mean temperature in coldspot Area	SHIn
1	1986	27.06	18.18	8.88
2	1998	28.49	18.05	10.44
3	2010	30.12	18.49	11.63
4	2017	32.82	1844	14.38

From 1986 to 2017, there was an increasing trend of spatial aggregation of high temperatures in the inner part of the urban zone and agriculture area (Figures 5.21, 5.22, 5.23 and 5.24). The Surface Heat Intensity (SHIn) estimated using hotspot analysis ranged between 8.8 °C and 14.38°C but exhibited clear trend between 1986 and 2017 (Table 5.11). Across all years, we did observed strong evidence of urban (built-up) area surface temperature being generally warmer than rural areas except agriculture land.

CHAPTER SIX

6. Conclusions and Recommendations

6.1 Conclusions

Rapid urban expansion in Hawassa has resulted not only in vast land cover dynamics but also associated changes in Surface Heat Intensity (SHIn).This research used a comprehensive approach combining supervise classification methods using maximum likelihood algorithm, linear regression and hotspot analysis using Getis-Ord Gi* statistics to investigate the relationship between land use land cover change and UHI effects.

The change detection method was working to quantify the spatial change of land use land cover units. In addition, statistical "from-to" information was applied to quantify the magnitude of change through the entire 30 year duration. Results confirmed that most distinct change was related to vegetation cover, swampy and agriculture land that decreased by an amount of 8.81%, 11.38% and 5.52% from 1986 to 2017 respectively. On the other hand, urban (built-up) areas, due to the construction of new industrial and commercial settlements, showed a considerable increase by 121.68%.These three land covers, agriculture lands, vegetation and swampy, were the main contributors to form new urban (built-up) areas. LST retrieve through Landsat satellite images is easily recognizable. Different algorithms were applied to the thermal infrared data of different Landsat images to accurately calculate LST of different land use land covers. Results showed that mean LST values were higher in agriculture lands and urban (built-up) areas than in the surroundings over the entire period. These anomalies were associated with settlements and industrial and commercial areas that experienced dense populations and the agricultural land cover by bare soils. Moreover, the most typical impact of rapid urbanization on LST was investigated within a single LULC. The change in LULC modified the radiant temperature of the surface. It was believed that the change in LST was strongly related to the removal of vegetation cover and swampy area their replacement with impressive surface. This can be concluded from the increase in the magnitude of LST by a rate of 3.65˚C in the entire period of study from 1986 to 2017. Based on the analysis of thermal pattern of the study area over the given period of time, the result of the study found gradual increase in temperature in urban (built-up) area. The study proved that the land surface temperature is influenced by the urbanization and agricultural land.

Results from remote sensing studies show that LST and land use land cover indices NDBI, NDVI and NDWI together can identify the pattern of temporal variation and spatial distribution in urban thermal environments. The highest NDBI was found in urban (built-up)

areas and agriculture lands while the highest NDVI was found in vegetation area and swampy. Statistical analysis showed that, the correlation between LST and NDBI was significantly high positive correlation. Whereas, NDVI was highly negative correlation with LST and NDWI also negative correlation with LST. By way of conclusion, the study area reveals comparatively higher LST and NDBI, and lower NDVI and NDWI over the period of study. The results indicated strong correlation between land surface temperature and Land use land cover indices. Other methods that investigated a regression analysis between LST and Land use land cover indices for each Land use land cover class also employed. This exhibited variations in the relationship depending upon the land use land cover types.

The study also revealed that hotspot analysis using Getis-Ord Gi* statistics was an appropriate method to examine changes in urban heat intensity patterns through time. In general, urban (built-up) area and agriculture lands of the study area found always warmer over a studied time table frame and water bodies, swampy and vegetation cover always revealed colder in the scope of the study time. Using Hotspots analysis calculate the surface heat intensity (SHIn) tends to increase through time SHIn 8.8°C in 1986,10.44°C in 1998, 11.63°C in 2010 and 14.38°C in 2017 and strongly correlated with urban expansion.

Over all observation of the study also discovered and highlighted the importance of intra-urban variation in thermal aggregation may also help in efficiently targeting area from the perspective of land use planning and urban management, it is recommend that the planners and policy makers should pay attention to the future land use policies and special considerations in planning corrective measures such as urban greening, publics space and treating the lack of Hawassa in the city land use land cover structure and in environment conservation policy.

6.2 Recommendations

The analysis of this study confirmed that, urban expansions in Hawassa town is in critical condition it is high time that concerned authorities take necessary initiatives and urban residents develop resilience to urban growth and UHI effect. However, it is suggested that the following limitations should be considered in future research. Use higher resolution imagery for land use land cover classification and it is better to take into account both day time and night time temperature data for more years, and need to assess other regression methods may give a better explanation of land use land cover composition-LST correlation as well as results that are more practical for urban planners.

On top of that, future studies need to explore detailed mechanisms for characterizing the relationship between surface temperature and land use land cover indices using different model and different factor like the direction and distance from the urban center and elevation. Understanding efficiency of various climate adaptation mechanisms and predicating the land surface temperature should also be the focus of future studies, and such knowledge may provide specific recommendations for urban planners and managers in relation to mitigation of urban heat intensity effects. The finding of the research are practical relevance for planning climate sensitive cities in Ethiopia.

Generally, more attention need to be given to environmental consequences of rapid urban expansions in developing countries. So that, the tropical warm climate need to be thoroughly investigated using a multidisciplinary approach.

References

Agarwal, C., Green, G. M., Grove, J. M., Evans, T. P., and Schweik, C. M. (2002). A review and assessment of land-use change models: dynamics of space, time, and human choice.

Al-Bakri, J.T., Dauqqah, M. and Brewer, T. (2013) Application of Remote Sensing and GIS for Modeling and Assessment of Land Use/Cover Change in Amman/Jordan. Journal of Geographic Information System, 5, 509-519.

Ali, H. (2009). Land use and land cover change, drivers and its impact: A comparative study from Kuhar Michael and Lenche Dima of Blue Nile and Awash Basins of Ethiopia (Doctoral dissertation, Cornell University).

Al Kuwari NY, Ahmed S, Kasiser MF (2016) Optimal Satellite Sensor Selection Utilized to Monitor the impact of urban Sprawl on the thermal Environment in Doha City, Quatar. J Earth climate change. 7:326.

Alhawiti, R.H. and Mitsova, D. (2016) Using Landsat-8 Data to Explore the Correlation between Urban Heat Island and Urban Land Uses. International Journal of Research in Engineering and Technology, 5, 457-466.

Almegdadi and Shuangao Wang. (2017). modelling urban sprawl Using remote sensed Data: A case study of Chennai city, Tamilnandu.

Anbar, M., (2012). The Climate impact on human comfort in the eastern Nile Delta. Journal of Faculty of Art, Cairo University, Vol. (72) no. 7, pp. 267–319.

Anderson et al. (1976). A land use and land cover classification system for use with remote sensor data.

Arizona Board of Regents. (2007). urban climate-climate study and UHI via the internet way back machine change: forcings, feedbacks, and the climate benefits of forests. Science. 320, 1444–1449.

Aronoff, S. (1989). Geographical Information System: A Management Perspective. WDL Publications: Ottawa.

Alexander Buyantuyev and Jianguo Wu, (2009) Urban Heat Islands and landscape heterogeneity: Linking spatio temporal variation in surface temperature to land cover and socioeconomic patterns.

Bernstein, L. S., Adler-Golden, S. M., Sundberg, R. L., Levine, R. Y., Perkins, T. C., Berk, A., ...Hoke, M. L. (2005).Validation of the Quick atmospheric correction (QUAC) algorithm for VNIR–SWIR multi- and hyper spectral imagery. SPIE proceedings,

algorithms and technologies for multispectral, hyper spectral, and ultra-spectral imager. SPIE Digital.

Birhan Asmame Miheretu and Assefa Abegaz Yimer. (2017).Land use/land cover changes and their environmental implications in the Gelanasub-watershed of Northern highlands of Ethiopia. Environmental System Research 6:7 DOI 10.1186/s40068-017-0084-7.

Burrough, A. (1986). Principles of Geographical Information Systems and Geo statistics. Oxford University Press: New York.

Buyadi, S. N. A., Mohd, W. M. N. W., and Misni, A. (2013). Impact of land use changes on the surface temperature distribution of area surrounding the National Botanic Garden, Shah Alam. Procedia-Social and Behavioral Sciences, 101, 516–525.

Burgan, R. E., and Hartford, R. A. (1993). Monitoring vegetation greenness with satellite data.

Buyantuyev, A. & Wu, J. (2009). Urban heat island and landscape heterogeneity: linking spatiotemporal variations in surface temperatures to land-cover and socioeconomic patterns. Landscape Ecology, 25(1): 17-33.

Chengbin Deng, Changshan Wu. (2013). examining the impacts of urban biophysical compositions on surface urban heat island: A spectral unmixing and thermal mixing approach Remote Sensing of Environment (262-274).

Chander, G. and Markham, B. (2003) Revised Landsat-5 TM Radiometric Calibration Procedures and Post calibration Dynamic Ranges. IEEE Transactions on Geoscience and Remote Sensing, 41, 2674-2677.

Chen, X., Zhao, H., Li, P., & Yin, Z. (2006). Remote sensing image-based analysis of the relationship between urban heat island and land use/cover changes. Remote Sensing of Environment, 104(2), 133-146.

Chintan P. Dave, Rahul Joshi and S. S. Srivastava, (2015).A Survey on Geometric Correction of Satellite Imagery. International Journal of Computer Applications, Volume 116 – No. 12.

Congalton, R. & Green, K. (2009). Assessing the accuracy of remotely sensed data. Principles and practices. Lewis Publishers, Boca Raton, Florida.137p.

Congalton, R.G. (1991). A Review of Assessing the Accuracy of Classifications of Remotely Sensed Data. Remote Sensing of Environment, 37, 35-46.

Dunn, C. P., Sharpe, D. M., Guntensbergen, G. R., Stearns, F., & Yang, Z. (1991). Methods for analyzing temporal changes in landscape pattern. In M. G. Turner & R. H.

Gardner (Eds.), Quantitative methods in landscape ecology: the analysis and interpretation heterogeneity (173-198). New York: Springer.

Dayawansa. (2003). Land suitability Identification for a production Forest through GIS technique.

Eastman, J.R. (2003) Guide to GIS and Image Processing 14, 239-247. Clark University Manual, USA.

Emilio Galdeano-Go´mez, (2008) Environmental performance and spillover effect on productivity: Evidence from horticulture firms. DOI: 10.1016/j.jenvman.2007.07.028.

ESRI. (2016). How Hot Spot Analysis (Getis-Ord Gi*) works, Last visit 17/10/2016, http://pro.arcgis.com/en/pro-app/tool-reference/spatial-statistics/h-how-hotspot-analysis-getis-ord-gi-spatial-stati.htm.

Evans, J.D. (1996). Straight forward statistics for the behavioral sciences. Pacific Grove CA: Brooks/Cole Publishing.

FAO. (2000) Land cover classification system. (http://www.fao.org/docrep/003/x0596e/x0596e01e.htm.)

Foody, G. (2002). Status of land covers classification accuracy assessment, Remote Sensing of Environment, 80, 185-201, 20.

Gillespie, A. (2014) Land Surface Emissivity. In: Njoku, E.G., Ed., Encyclopedia of Earth Sciences Series—Encyclopedia of Remote Sensing, Springer, New York. https://doi.org/10.1007/978-0-387-36699-9 Library.

Gao, J. (2009). Digital Analysis of Remotely Sensed Imagery. McGraw-Hill Companies, Inc., New York.

Getter, K.L, Rown, D.B., (2006). The role of extensive green roofs in sustainable development. Hort Science 41, 1276-1285.

Guo, G., Wu Z, Xiao, R, Chen Y., X., Zhang, X. (2015). Impact of Urban biophysical composition on land surface Temperature in urban heat island cluster. Landscape Urban Planning 135, 1-10.

Gudina, I. Feyissa, Henrik Meilby, G. Darrel Jennerette, Stephen Pauliet. (2016).Locally optimized separability enhancement induce for urban land cover mapping: Exploring thermal environment consequences of rapid urbanization in Addis Ababa, Ethiopia. Remote Sensing of Environment 175(2016) 14-31.

J. A. Sobrino, Raissouni and Zhao-Liang Li, (2001). A Comparative Study of Land Surface Emissivity Retrieval from NOAA Data. Remote sensing of Environment PII S0034 4257(00)00171-1.

J. Tangl Wang and Z. Yao. (2007). Spatio-temporal urban landscape change analysis using the Markov chain model and a modified genetic algorithm: International Journal of Remote sensing, Vol.28, 3255-3271.

Jensen, J.R. (2005). Introductory Digital Image Processing: A Remote Sensing Perspective.3rd ed. Prentice Hall, Upper Saddle River, NJ.

Jensen, J.R. (2016) Introductory Digital Image Processing: A Remote Sensing Perspective. No. Ed. 4, Prentice-Hall Inc., Upper Saddle River.

Herold, M., Goldstein, N. C., & Clarke, K. C. (2003). The spatiotemporal form of urban growth: Measurement, analysis and modeling. Remote sensing of Environment, 86, 286-302.

Kim, H. H., 1992, Urban Heat Island, International Journal of Remote Sensing, 13 (12), 2319-2336.

Landis, J.R. and Koch, G.G. (1977) A One-Way Components of Variance Model for Categorical Data. Biometrics, 33, 671-679.

Linli Cuia, Jun Shi b, (2012). Urbanization and its environmental effects in Shanghai, China. Urban Climate (1-15).

Li, L., Tan, Y., Ying, S., Yu, Z., Li, Z. and Lan H. (2014) Impact of Land Cover and Population Density on Land Surface Temperature: Case Study in Wuhan, China. Journal of Applied Remote Sensing, 8, 1-19.

Lillesand, T., Kiefer, R. W, and Chipman, J. (2014). Remote sensing and image interpretation. John Wiley and Sons, New Delhi.

Lillesand, T., Keifer, R.W., and Chipman, J. (2007). Remote Sensing and Image Interpretation (Sixth Edition), Wiley, Hoboken, USA.

Liu, L., Zhang, Y., 2011. Urban heat island analysis using the Landsat TM data and ASTER data: A case study in Hong Kong. Remote Sens. 3, 1535–1552.

Legendre, P., & Fortin, M. J. (1989).Spatial pattern and ecological analysis. Vegetation, 80,107-138.

McFeeter, (1996). The use of Normalized Difference Water Index (NDWI) in the Delineation of open water feature 1425-1432.

McGregor, G. R., & Nieuwolt, S. (1998).Tropical climatology (2nd ed.). Chichester, England: John Wiley & Sons, Ltd.

Mendelbrot, B. B. (1983).The fractal geometry of nature. New York: W.H. Freeman and Company.

Malczewski, J. (1999). GIS and Multi criteria Decision Analysis. New Analysis. New York: John Weily and Sons. Inc.

McGregor, G. R., & Nieuwolt, S. (1998).Tropical climatology (2nd ed.). Chichester, England: John Wiley & Sons, Ltd.

Michael Heinla, Albin Hammerlea, Ulrike Tappeinera, Georg Leitinger. (2015).Determinates of urban-rural land surface temperature difference- A landscape scale perspective. Landscape and urban planning, (33-42).

Naissan and Lily, (2016) Aesthetic Dermatology: Effect of climate change on skin. www.mdedge.com/edermatolgynews/.

Nguyen Hoang Khanh Linh, Huynh Van Chuong. (2015).Assessing the Impact of Urbanization on Urban Climate by Remote sensing Perspective, A case study in Danag City, Vitnam, the international archive of photogrammetry, remote sensing and spatial Information Sciences, Volume XL-7/W3,207-212.

Ndeyeb Yacine Barry, Vieux Boukhaly Traore, Mamadou Lamine Ndiaye4, Osemwegie Isimemen1, Hauhouot Celestin1, Bienvenu Sambou2(2017)Assessment of Climate Trends and Land Cover/Use Dynamics within the Somone River Basin, Senegal American Journal of Climate Change, 2017, 6, 513-538.

Nemani, R. R., and Running, S. W, (1989). Estimation of regional surface resistance to evapotranspiration from NDVI and thermal-I R A VHRR data. Journal of Applied Meteorology, 28, 276– 284.

Ord, J. K., and Getis, A. (1995).Local spatial autocorrelation statistics—Distributional issues and application. Geographical Analysis, 27,286–306.

Omran, E.S.E. (2012) Detection of Land-Use and Surface Temperature Change at Different Resolutions. Journal of Geographic Information System, 4, 189-203.

Peiju Du, Pei Liu, Junshi Xia, Li Feng Sicong Liu, Kun Tan and Liang Cheng. (2014). Remote sensing Image Interpretation for Urban Environment Analysis: Methods, system and Examples.

Q. WENG. (2001).Remote sensing – GIS evaluation of urban expansion and its impact on surface temperature in the Zhujiang Delta, China International Journal of Remote Sensing.Vol.22,1999-2014.

Qihao Weng, Jacquelyn Schubring. (2004). Estimation of land surface temperature–vegetation abundance relationship for urban heat island studies, Remote Sensing of Environment 89, 467 – 483.

Qihao Weng. (2012). remote sensing of impervious surfaces in the urban areas: Requirements, methods, and trends Remote Sensing of Environment. (34-49).

Qijiao Xie, Zhixiang Zhou. (2015). Impact of urbanization on urban heat Island Effect Based on TM Imagery In Wuhan, China, China Environmental Engineering and Management Journal March 2015, Vol.14, No. 3, 647-655.

Roger A. Pielke S r, Gregg Marland, Richard A. Betts, Thomas N. Chase, Joseph L. Eastman, J o h n O. Niles, Devdutta S. NiyogI, and Steven W. Running.(2002). The influence of land-use change and landscape dynamics on the climate system: relevance to Climate-change policy beyond the radioactive effect of greenhouse gases.

Rajender Kumar Mehta. (2011). Land Use Land Cover Change Detection Using Remote Sensing Data and GIS Tools: A Case Study of Delhi State.

Rajchandar Padmanaban, Avit K. Bhowmik, Pedro Cabral, Alexander Zamyatinb, Oraib Won Hoi Hwang. (2007). Estimation of the Effects of Vegetation on Local Climate Using GIS and Remote Sensing Data.

Raman Maini and Himanshu Aggarwal. (2010).A Comprehensive Review of Image Enhancement Techniques. Journal of computing, volume 2, ISSN 2151-9617.

Ridd, M.K. and Liu, J. (1998) A Comparison of Four Algorithms for Change Detection in an Urban Environment. Remote Sensing of Environment, 63, 95-100.

Richards, J. and Jia, X. (2006). Remote Sensing Digital Image Analysis: An Introduction. Springer, Berlin Springer-verglag.

Roth, M. (2007).Review of urban climate research in (sub) tropical regions. International Journal of Climatology, 27, 1859–1873.

Sophia S. Rwang, J.M. Ndambuki Accuracy Assessment of Land Use/Land cover classification Using Remote Sensing and GIS.

Srivanit, M., Hokao, K., & Phonekeo, V. (2012). Assessing the Impact of Urbanization on Urban Thermal Environment: A Case Study of Bangkok Metropolitan, International Journal of Applied Science and Technology, 2(7), 243-256.

Sk. Morshed Anwar. (2002). Land Use change Dynamics: A Dynamics Spatial Simulation.

S. Ahmed. (2017). Assessment of urban heat islands and impact of climate change on socioeconomic over Suez Governorate using remote sensing and GIS techniques. The Egyptian Journal of Remote Sensing and Space Sciences.

Shannon, C., & Weaver, W. (1964). The mathematical theory of communication. Urbana: University of Illinois Press.

Samwel N. Marigi. (2017). Climate Change Vulnerability and Impacts Analysis in Kenya American Journal of Climate Change, 6, 52-74.

Stewart, I. D., and Oke, T.R. (2012).Local climate zones for urban temperature studies. American Meteorological Society, 93, 1879–1900.

Thomas M. Lillesad. Ralph W.Kifer. Jonathan W.Chipman Remote Sensing and Image and Image Interpretation.

Tran Hunga,*, Daisuke Uchihama b, Shiro Ochib, Yoshifumi Yasuoka. (2006). Assessment with satellite data of the urban heat island effects in Asian mega cities International Journal of Applied Earth Observation and Geoinformation, 34–48.

Shukla, J., Nobre, C., and Sellers, P. (1990). Amazon deforestation and climate change. Science (Washington), 247(4948), 1322–1325.

S. Ahmed. (2017).Assessment of urban heat islands and impact of climate change on socioeconomic over Suez Governorate using remote sensing and GIS techniques. The Egyptian Journal of Remote Sensing and Space Sciences http://dx.doi.org/10.1016/j.ejrs.2017.08.001.

Van, T.T., Bao, H.D.X., 2010. Study of the impact of urban development on surface temperature using remote sensing in Ho Chi Minh City, North Vietnam. Geographical Res. 48 (1), 86–96.

Walsh, C. L, Dawson, R. J, Hall, J. W, Barr, S. L, Batty, M., Bristow, A. L, and Tight, M.R. (2011). Assessment of climate change mitigation and adaptation in cities. Proceedings of the Institution of Civil Engineers-Urban Design and Planning, 164(2), 75–84.

Weng Q., and Larson R.C., 2005. 10 satellite remote sensing of urban heat islands: current practice and prospects.

Weng, Q., Lu, D., and Schubring, J. (2004). Estimation of land surface temperature–vegetation abundance relationship for urban heat island studies. Remote sensing of Environment, 89(4), 467–483.

Weng, Q. H. (2012).Remote sensing of impervious surfaces in the urban areas: Requirements, methods, and trends. Remote sensing of Environment, 117, 34–49.

Weng, Q. (2001).A remote sensing-GIS evaluation of urban expansion and its impact on surface temperature in the Zhujiang delta, China. International Journal of Remote Sensing, 22, 1999–2014.

Weng, Qihao. (2012). remote sensing of impervious surface in the urban areas: requirements, methods, and trends. Remote Sensing of Environment 117, 34-49.

Wilson, J.S., Clay, M., Martin, E., Stuckey, D. and Vedder-Risch, K. (2003). Evaluating Environmental Influences of Zoning in Urban Ecosystems with Remote Sensing. Remote Sensing of Environment, 86, 303-321.

Weng and Larson, (2005) Satellite remote sensing of urban heat island: current practice and prospects DOI: 10.1007/3-540-26676-3_10.

Wu, J., Jelinski, E. J., Luck, M., and Tueller, P. T. (2000). Multi scale analysis of landscape heterogeneity: Scale variance and pattern metrics. Geographic Information Sciences, 6, 6–19.

Xiong, Y., Huang, S., Chen, F., Ye, H., Wang, C. and Zhu, C. (2012). The Impacts of Rapid Urbanization on the Thermal Environment: A Remote Sensing Study of Guangzhou, South China. Remote Sensing, 4, 2033-2056.

Yue, W., Xu, J., Tan, W., and Xu, L. (2007). The relationship between land surface temperature and NDVI with remote sensing: application to Shanghai Landsat 7 ETM+ data. International Journal of Remote Sensing, 28(15), 3205–3226.

Zanter, K. (2016) Landsat 8 (L8) Data Users Handbook. LSDS-1574 Version 2, 1-106.

Zaksek, K., and Ostir, K. (2011). Downscaling land surface temperature for urban heat island diurnal cycle analysis. Remote Sensing of Environment, 115, 114-124.

Zhu, S., & Zhang, G. (2011, October). Analysis on Relationship between Urban Land Surface Temperature and Land cover from Landsat ETM+ Data. In: Proc. of Fourth International Symposium on Knowledge Acquisition and Modeling, IEEE, Sanya, China.

Zha, Y., Gao, J., Jiang, J., Lu, H., and Huang, J. (2012). Normalized difference haze index: a new spectral index for monitoring urban air pollution. International journal of remote sensing, 33(1), 309–321.

Zha, Y., Gao, J. and Ni, S. (2003). Use of Normalized Difference Built-Up Index in Automatically Mapping Urban Areas from TM Imagery. International Journal of Remote Sensing, 24, 583-59.